**SANDIA REPORT**
SAND2012-0132
Unlimited Release
Printed November 2011

# Nanotexturing of Surfaces to Reduce Melting Point

David Zubia, Stella Quinones, Jose Mireles, Noel Marquez, and Ernest J Garcia

Prepared by
Sandia National Laboratories
Albuquerque, New Mexico 87185 and Livermore, California 94550

Sandia National Laboratories is a multi-program laboratory managed and operated by Sandia Corporation, a wholly owned subsidiary of Lockheed Martin Corporation, for the U.S. Department of Energy's National Nuclear Security Administration under contract DE-AC04-94AL85000.

Approved for public release; further dissemination unlimited.

Issued by Sandia National Laboratories, operated for the United States Department of Energy by Sandia Corporation.

**NOTICE:** This report was prepared as an account of work sponsored by an agency of the United States Government. Neither the United States Government, nor any agency thereof, nor any of their employees, nor any of their contractors, subcontractors, or their employees, make any warranty, express or implied, or assume any legal liability or responsibility for the accuracy, completeness, or usefulness of any information, apparatus, product, or process disclosed, or represent that its use would not infringe privately owned rights. Reference herein to any specific commercial product, process, or service by trade name, trademark, manufacturer, or otherwise, does not necessarily constitute or imply its endorsement, recommendation, or favoring by the United States Government, any agency thereof, or any of their contractors or subcontractors. The views and opinions expressed herein do not necessarily state or reflect those of the United States Government, any agency thereof, or any of their contractors.

Printed in the United States of America. This report has been reproduced directly from the best available copy.

Available to DOE and DOE contractors from
U.S. Department of Energy
Office of Scientific and Technical Information
P.O. Box 62
Oak Ridge, TN 37831

Telephone: (865) 576-8401
Facsimile: (865) 576-5728
E-Mail: reports@adonis.osti.gov
Online ordering: http://www.osti.gov/bridge

Available to the public from
U.S. Department of Commerce
National Technical Information Service
5285 Port Royal Rd.
Springfield, VA 22161

Telephone: (800) 553-6847
Facsimile: (703) 605-6900
E-Mail: orders@ntis.fedworld.gov
Online order: http://www.ntis.gov/help/ordermethods.asp?loc=7-4-0#online

SAND2012-0132
Unlimited Release
Printed November 2011

# Nanotexturing of Surfaces to Reduce Melting Point

David Zubia, Stella Quinones, and Noel Marquez
Department of Electrical and Computer Engineering
University of Texas at El Paso
El Paso, TX 79968

Jose Mireles
Instituto de Ingenriería y Tecnología
Universidad Autónoma de Ciudad Juárez
Ciudad Juárez, Mexico

Ernest J. Garcia
Electromechanical Engineering Department
Sandia National Laboratories
P.O. Box 5800
Albuquerque, New Mexico 87185-1064

**Abstract**

This investigation examined the use of nano-patterned structures on Silicon-on-Insulator (SOI) material to reduce the bulk material melting point (1414 °C). It has been found that sharp-tipped and other similar structures have a propensity to move to the lower energy states of spherical structures and as a result exhibit lower melting points than the bulk material. Such a reduction of the melting point would offer a number of interesting opportunities for bonding in microsystems packaging applications. Nano patterning process capabilities were developed to create the required structures for the investigation. One of the technical challenges of the project was understanding and creating the specialized conditions required to observe the melting and reshaping phenomena. Through systematic experimentation and review of the literature these conditions were determined and used to conduct phase change experiments. Melting temperatures as low as 1030 °C were observed.

# CONTENTS

# FIGURES

# TABLES

# ACRONYMS

| | |
|---|---|
| BOE | Buffered Oxide Etch |
| COMS | Commercialization of MEMS conference |
| CVD | Chemical Vapor Deposition |
| 3D | Three-Dimensional |
| dB | Decibel |
| DC | Direct Current |
| DI | Deionized Water |
| DOE | Department of Energy |
| EDAX | Energy dispersive x-ray spectroscopy |
| LEL | Lower Explosive Limit |
| MBE | Molecular Beam Epitaxy |
| MEMS | Microelectromechanical Systems |
| MOCVD | Metalorganic Chemical Vapor Disposition |
| NIL | Nanoimprint lithography |
| RCA | Radio Corporation of America |
| RIE | Reactive Ion Etcher |
| SEM | Scanning Electron Microscope |
| S-FIL/R | Step and Flash Imprint Lithography with Tone Reversal |
| SI | Silicon |
| SNL | Sandia National Laboratories |
| SOI | Silicon on Insulator |
| UACJ | Universidad Autónoma de Ciudad Juárez |
| UTEP | University of Texas at El Paso |
| UHP | Ultra High Purity |
| XRD | X-Ray Diffraction |

# 1. INTRODUCTION

This was a 3 year collaborative project between University of Texas at El Paso (UTEP), Universidad Autónoma de Ciudad Juárez (UACJ) and Sandia National Laboratories (SNL) to study and use reduced melting of *nano*-patterned silicon for microsystems applications such as for bonding of surfaces. During the project it was discovered that a more general and useful three-dimensional (3D) morphological transformation of *micro*-patterned silicon was possible under special annealing conditions. Experiments were systematically performed to replicate the reduced melting point and three-dimensional (3D) morphological transformation. In the process of this three year project, extensive research capability was created at UTEP and UACJ including dry etching, lithography, annealing and design. A total of four students were supported; one master and one baccalaureate student were graduated during the period. The master student successfully presented his master's thesis.

One of the technical challenges of the project was understanding and creating the specialized conditions required to observe the melting and reshaping phenomena. Through systematic experimentation and review of the literature, the researchers were able to determine that high temperature (>960C) in an extremely pure ambient with hydrogen and free of oxygen or alternatively in a high-vacuum (<10-8 Torr) was crucial. These conditions are usually created by expensive Molecular Beam Epitaxy (MBE) or Metalorganic Chemical Vapor Deposition (MOCVD) systems, thus it was difficult to replicate them given the degree of purity and hazard of working in a hydrogen ambient. In conclusion, a custom heating chamber was created. Results from the custom heating chamber were encouraging in terms of the purity required; however, the necessary temperature of at least 960C was not achieved in the initial trials. More work was needed to increase the temperature.

Other challenges associated with creating the nano and micro-patterned silicon and SOI wafers were met. This project successfully created processes for nano-patterning of silicon via collaboration between UTEP, UACJ and University of Texas at Austin. Moreover, the micro-patterning was collaboratively and successfully performed at UTEP and UACJ.

Work was performed at UACJ on the design and simulation of chevron actuators including the fabrication of a lithography mask. The purpose of this work was to heat the chevron arms with electrical current to induce rounding of the tubular arms. This work was created and simulated with Coventor software and predicted sufficient heating of the arms with applied voltage bias.

In summary, this project created research capacity at UTEP, mentored four students and graduated two, produced a master's thesis and, strengthened collaborations with UACJ in Mexico.

## 1.1 Technical Background

Particles with nanometer dimensions contain a significant fraction of the total number of atoms at the surface, and as a consequence, the surface can have a significant effect on the thermodynamic properties of a phase and vice versa. The extensive thermodynamic properties (where extensive refers to properties which depend on the extent or mass of the system) of a

phase will include contributions which depend on the nature of its surface. [1] The total Gibbs free energy of a system can therefore be partitioned into volume and surface contributions [2, 3] $G = VG_v + AG_s$, where $G_S$ is the surface specific free energy, $A$ is the surface area, $G_v$ is the free energy per unit volume and, $V$ is the volume. The total surface free energy, $AG_s$, in a nanoscale particle can be significant.

For instance, for a given volume, phases will try to lower their free energy by changing their shape according to the criterion [4], $\int \gamma(\mathbf{n})dA = \min\text{imum}$, where $\gamma$ is the surface tension, and $\mathbf{n}$ is the surface unit normal. In a liquid, $\gamma$ is isotropic therefore the minimum free shape corresponds to the shape with the minimum surface area which is a sphere. For a solid, the broken bond density will vary as a function of crystal surface orientation causing $\gamma$ to also vary with orientation. In face-centered cubic crystals the surfaces with the lowest $\gamma$ are the close-packed planes and this will influence the shape of small crystals. Conversely, the shape of a surface can influence the internal energy and thermodynamic properties of a particle. In order to see this, consider a closed system in which a liquid droplet of radius $r$ is in equilibrium with its vapor pressure, under the conditions of no external gas pressures, and zero surface tension. In this system, the equilibrium pressure in the interior of a liquid droplet is equal to the equilibrium vapor pressure, $P_{in}^{eq} = P_{ex}^{eq}$ where $P_{in}$ is the pressure inside the liquid and $P_{ex}$ is the vapor pressure. If the surface tension is now allowed to have a nonzero value ($\gamma \neq 0$), the pressure in the liquid will change by an amount $2\gamma/r$. However, in order for the system to maintain equilibrium, the changes in the Gibbs free energies of the liquid and vapor must be equal according to the Gibbs-Thomson equation, $kT \ln \frac{P_{ex}}{P_{ex_O}} = \frac{2\gamma\Omega}{r}$, where $P_{exo}$ describes the pressure when $\gamma = 0$. Thus the vapor pressure increases to maintain thermodynamic equilibrium. This example demonstrates that the size (radius) of a particle influences the equilibrium vapor pressure. The Gibbs-Thomson equation can be generalized to curved solid surfaces where $\gamma$ is isotropic. In this case the chemical potential along the surface is dictated by the surface profile according to [5] $\mu(x,y) = \mu_o + \gamma\Omega\kappa(x,y)$, where $\mu_o$ is the chemical potential in the bulk away from the interface, and $\kappa$ is the curvature of the surface. If the surface has a sinusoidal profile given by $z_s(x) = A\sin Kx$ as shown in Figure 1, where $A$ is the amplitude and $K$ is the period, then the curvature is given by

$$\kappa(x) = -\frac{\partial^2 z_s / \partial x^2}{\left\{1 + \left(\partial z_s / \partial x\right)^2\right\}^{3/2}} = \frac{AK^2 \sin Kx}{\left\{1 + \left(AK\cos Kx\right)^2\right\}^{3/2}}.$$

Thus a sinusoidal surface profile gives rise to a varying chemical potential at the surface with same period and phase as the surface profile. The use of a sinusoidal surface profile is convenient because an arbitrary periodic profile can be reconstructed using a Fourier series of sinusoidal waves. These surface thermodynamic effects are important in explaining some of the phenomenological effects observed in nanometer size particles such as the reduction of melting point and mass transport of small nuclei.

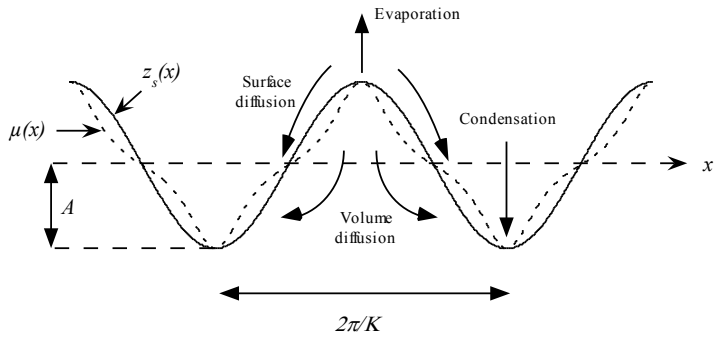


**Figure 1. Modulation of chemical potential attributed to surface curvatuve.**

One important thermodynamic property that is affected by size is melting point. The melting temperature of small particles has been shown to decrease as the particle size decreases according to the relation [6], $\Delta T = c/r$, where $\Delta T$ is the change in the melting temperature and, $c$ is a constant of proportionality. Several phenomenological models have been proposed to account for this effect. One model proposed by Peppiatt and Sambles [6] is the liquid skin model. In this model, a solid melts by the formation of a liquid skin covering the particle. A liquid skin, once formed, is able to progress through the solid without requiring an activation energy. The temperature, $T_{sk}$, at which the liquid skin is formed is given by [6]

$$T_o - T_{sk} = \frac{2T_o}{100\Delta H_m \rho_{Sm} r}\left\{\gamma_{SL} + \left(1 - \frac{\rho_S}{\rho_L}\right)\gamma_L\right\}$$

where $r$ (cm) is the radius of the particle or the radius of curvature of a morphological feature, $T_o$ (°C or K) is the bulk melting point, $\Delta H_m$ (J/mol) is the heat of melting, $\rho_S$ (g/cm$^3$) is the density of the solid, $\rho_{sm}$ (mol/cm$^3$) is the molar density of the solid and $\rho_L$ (g/cm$^3$) is the density of the liquid. $\gamma_{SL}$ and $\gamma_L$ are in units of N/cm.

## 1.2 Preliminary Results

The melting temperature of silicon as a function of temperature predicted by Peppiatt and Sambles model is plotted in Figure 2. The values used for the calculation in Figure 2 are $T_o$ = 1410 °C, $\Delta H_m$ = 50.2*10$^3$ (J/mol), $\rho_S$ = 2.53 (g/cm$^3$), $\rho_{sm}$ 0.082 (mol/cm$^3$), $\rho_L$ = 2.53 (g/cm$^3$), $\gamma_{SL}$ = 3.6*10$^{-3}$ (N/cm), and $\gamma_L$ = 7.2*10$^{-3}$ (N/cm).

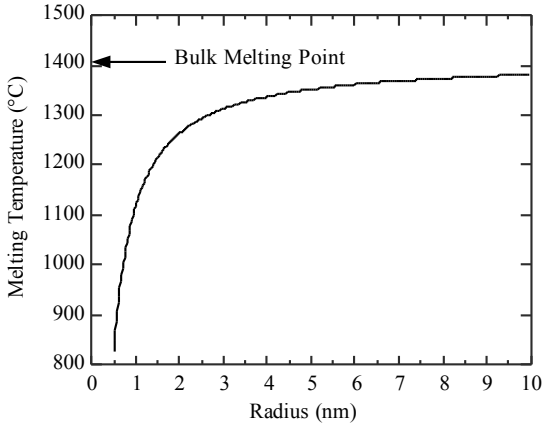


**Figure 2. Predicted melting temperature of silicon as a function of size using the liquid skin model.**

Preliminary experiments have shown that indeed the melting point of nanosized silicon is reduced. For example, evidence of reduced melting point in silicon is shown in Figure 3 which compares the size and shape of silicon nanometer sized islands after heat treatment at (a) 996 °C and (b) 1055 °C for 10 minutes under a hydrogen/nitrogen environment. Figure 3(b) shows that a gross morphological change has occurred in the sample heated to 1055 °C while the sample heated to 996 °C shows very sharp features similar to non-heat treated samples.

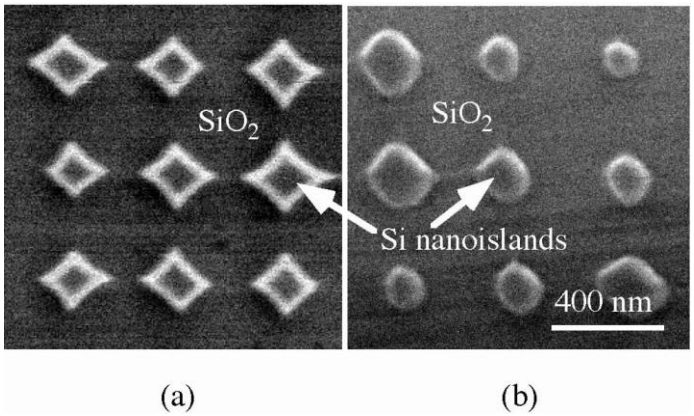


**Figure 3. Plan view SEM images of nanostructured SOI after heating at (a) 996 °C and (b) 1055 °C**

In the literature, several criteria have been used to determine the melting point including; the disappearance of the state of order in the solid, the sharp variation of some physical properties and the sudden change in the particle shape. [7] One possible explanation for this gross morphological change is that the melting point for these nanostructured silicon islands was reduced from its bulk value of 1412 ˚C to less than 1025 ˚C. As discussed above, a reduction in melting point is anticipated in nanophase materials. [8] However, it is estimated from the graph of calculated silicon melting temperature versus particle size (see Figure 2) that for a melting temperature of 1025 °C the particle size would have to be roughly 0.8 nm. The size of the silicon nanoislands in 3(a) are much larger at ~100 nm in diameter and ~40 nm in thickness, thus the reduction in the melting temperature in these nanoislands is not explained by the size. However

close inspection of the shape of the nanoislands in 3(a) reveals that they contain very sharp features. As suggested by the theoretical discussion above, the reduction in melting temperature in these nanoislands could be explained to be controlled by the radius of curvature of the morphological features although the small size of the islands helps to destabilize the phase.

## 1.3 Technical Approach

In this project, silicon surfaces were nanostructured using interferometric (or holographic) lithography and reactive ion etching [9, 10] to form 2-dimensional arrays. Interferometric lithography is a simple and inexpensive method to fabricate periodic nanoscale structures. Interference effects between two coherent laser beams are used to produce simple periodic patterns with periodicity given by [9] $d = \lambda/(2\sin\theta)$, where $\lambda$ is the wavelength of the exposing beams and $2\theta$ is the angle between the two intersecting beams. The experimental configuration used for recording the patterns is illustrated in Figure 4. The sample and a mirror are mounted at right angles on a rotation stage causing the two incident beams on the sample to intersect at an angle $2\theta$. Rotation of the stage allows $\theta$ to be adjusted. This creates an interference pattern on the sample with periodicity governed by $d = \lambda/(2\sin\theta)$. The interference pattern is then recorded using photoresist and then transferred into the substrate using a reactive-ion-etch processing sequence.

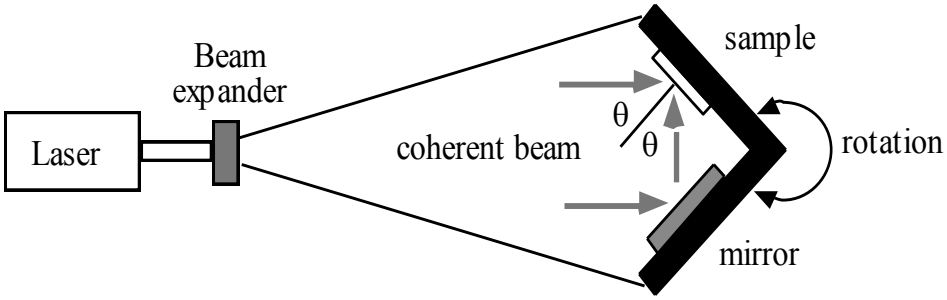


**Figure 4. Interferometric setup for recording periodic patterns on the substrate.**

# 2. EXPERIMENTAL RESULTS

Initial experiments were focused on observing a reduced melting point effect and later experiments transition towards exploiting the surface transformation through hydrogen annealing. While the general methods and strategies used by other researchers to reshape silicon show a successful outcome for silicon reshaping by hydrogen annealing, most of these experiments were performed on multi-million dollar Chemical Vapor Deposition (CVD) or related equipment. This report will cover sample fabrication, sample cleaning, annealing experimentation, and equipment design considerations. The experiments hereby presented are an exploration of the requirements for both reduced melting point, and silicon surface transformation by hydrogen annealing. The fabrication of the nano- and micro-structures is presented first. This is followed by discussion of various methods used to heat-treat the structures and results from the heating. Finally, designs and simulation of Microelectromechanical Systems (MEMS) test structures that can be used to study the reshaping of silicon are presented.

## 2.1 Pattern Fabrication

To explore the reshaping effect, silicon wafers were patterned. The wafers patterned were p-type, (100) orientation both 3 and 4 inch in silicon and silicon on insulator (SOI). Two main types of patterns will be discussed in this section: nano-sized, and micro-sized.

### *2.1.1 Nanopatterning*

Nanoscale patterning cannot be performed with the traditional photolithography methods. In this case, the pattern was done through nanoimprint lithography (NIL) on an IMPRIO 100 machine from Molecular Imprints Inc., which is capable of submicron scale patterning. Both Si and SOI (100) wafers were processed by NIL as illustrated in Figure 5. This work was performed by Dr. Zubia and Noel Marquez at the University of Texas at Austin.

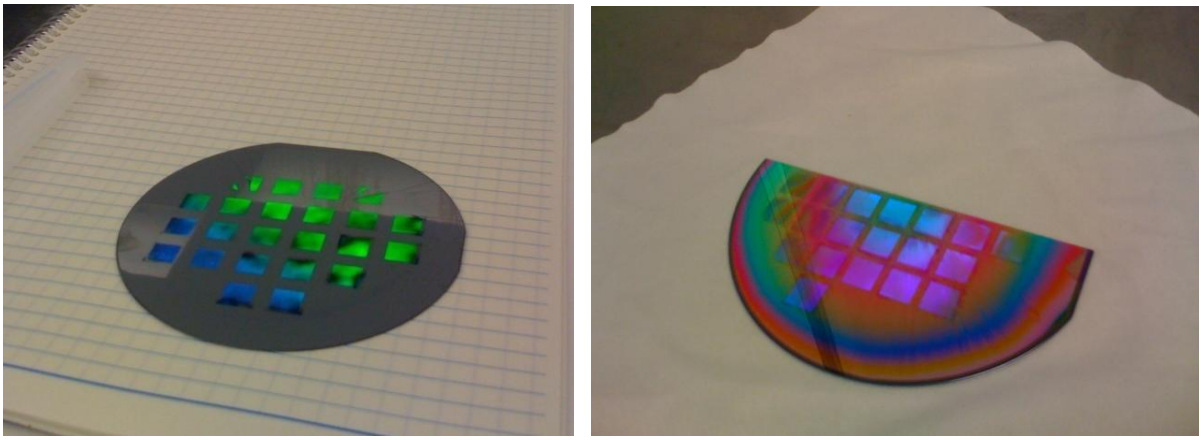

**Figure 5. Optical images of (a) NIL patterned Si wafer and (b) NIL patterned SOI wafer.**

The particular technique used to pattern these wafers was step-and-flash imprint lithography with tone reversal (S-FIL/R). A rough outline of this procedure is as follows:

1. Wafer cleaning. Standard Radio Corporation of America (RCA) clean or piranha + Buffered Oxide Etch (BOE).
2. A UV curable, low viscosity polymer is used to coat the wafer.
3. A transparent, hard mold is pressed on to the area to be patterned and subsequently illuminated with UV light to cure the polymer.
4. A silicon containing monomer (SilSpin) is used to coat the imprinted region to serve as a planarization layer.
5. The silspin is etched and planarized to the level of the imprints using an $O_2$ + $CHF_3$ plasma on a Reactive Ion Etcher (RIE) system.
6. The monomer is etched to expose the silicon substrate using $O_2$ + Ar.
7. The silicon is anisotropically etched using $Cl_2$ + HBr to de desired depth
8. The wafer is isotropically etched using $SF_6$ to achieve the desired size.

Additionally, SOI wafers may be thinned to the desired thickness before patterning through SF6 dry etching. The mask used has a rectangular array of circles with a center-to-center distance of 400 nm and a radius of 150 nm covering an area of 1 $cm^2$. The complete procedure is illustrated in Figure 6 and Figure 7.

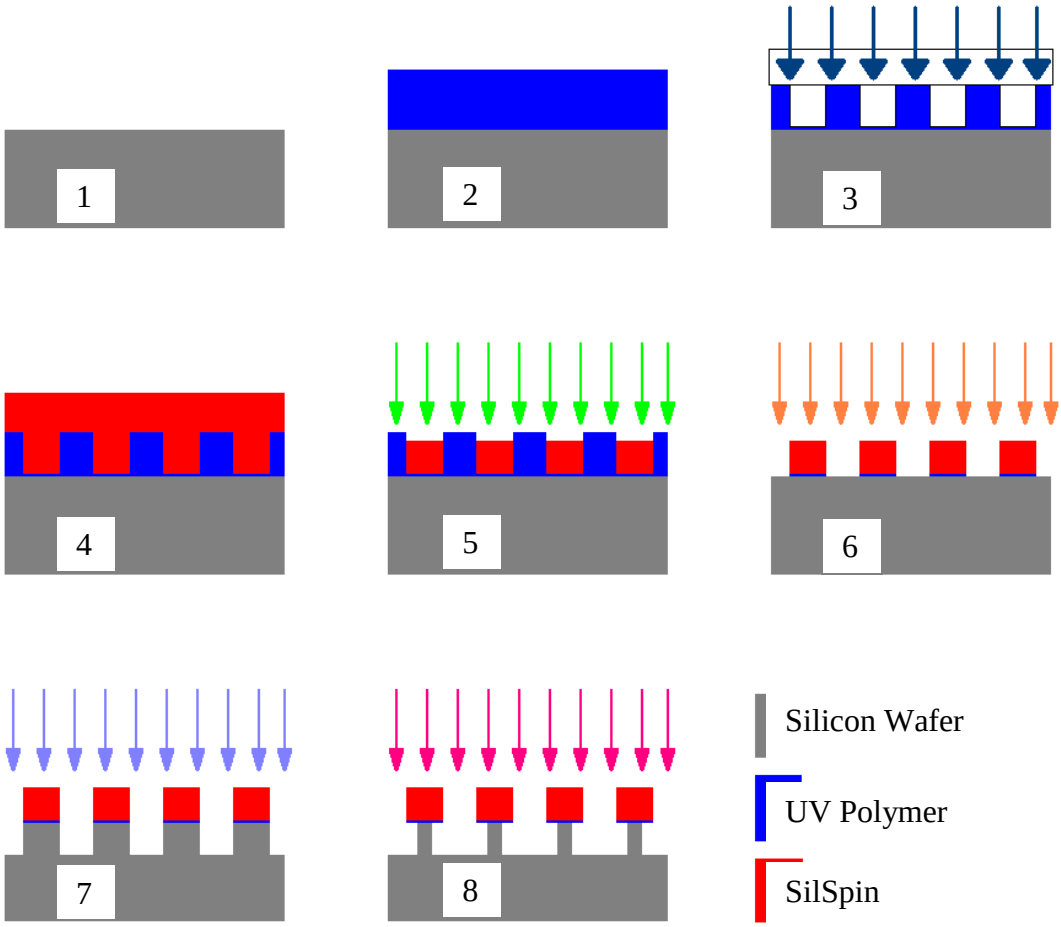


**Figure 6. Nanoimprint lithography process steps (cross sectional view): 1. clean, 2. Polymer coat, 3. UV cure, 4. Silspin coat, 5. O2 + CHF3 etch, 6. O2 + Ar etch, 7. Cl2 + HBr etch,. 8. SF6 etch.**

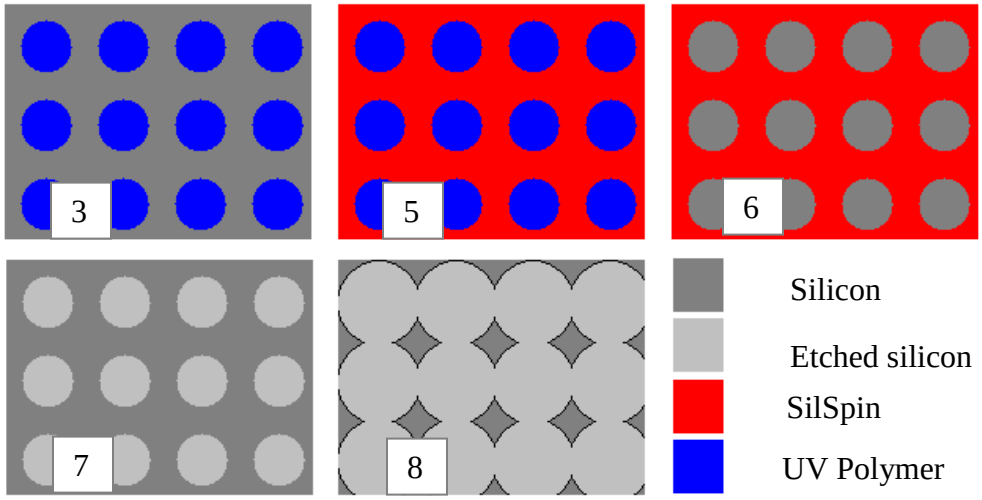


**Figure 7. Selected steps for Nanoimprint lithography, top view (SilSpin omitted on 7 & 8).**

The remaining Silspin and polymer can be dry etched or removed with a chemical cleaning step. The resulting pattern for silicon wafers is illustrated in Figure 8.

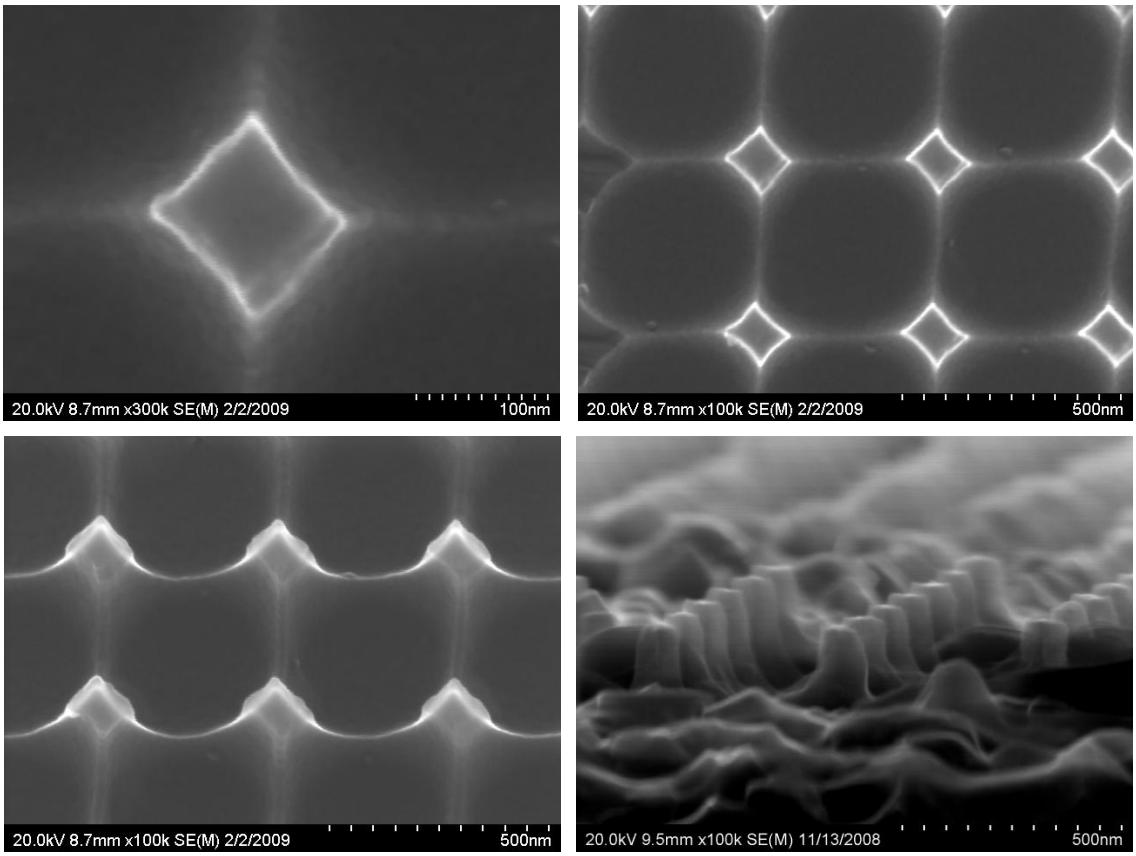


**Figure 8. Various views of NIL patterned silicon samples.**

Due to equipment issues, some of the samples did not go through the regular etching steps at U.T. Austin and had to be finished at UTEP. Depending on the etching needed and materials available, appropriate steps were taken for different samples. Etching was performed on a Plasmalab 80 Plus reactive ion etcher (RIE) from Oxford. The Plasmalab was installed at UTEP by Noel Marquez during the project period and is shown in Figure 9. This included installation of $SF_6$ capability. The etch process was also developed by Noel Marquez.

**Figure 9. Oxford Plasmalab 80 Plus RIE.**

Silicon wafer-1 was processed up to step 7 (up to SilSpin removal) at UT Austin. $SF_6$ was not available at UTEP, therefore etching was done with $CF_4$, $O_2$ and Ar using the parameters listed in Table 1. Estimated etch rate in the x/y plane was 25 nm/min. The etched silicon wafer is shown in Figure 10.

**Table 1. Etch parameters used for a silicon wafer.**

| **Parameter** | **Value** | **units** |
|---|---|---|
| Pressure | 0.05 | Torr |
| Power | 200 | Watts |
| Time | 4 | Minutes |
| $CF_4$ | 30 | Sccm |
| Ar | 10 | Sccm |
| $O_2$ | 10 | Sccm |

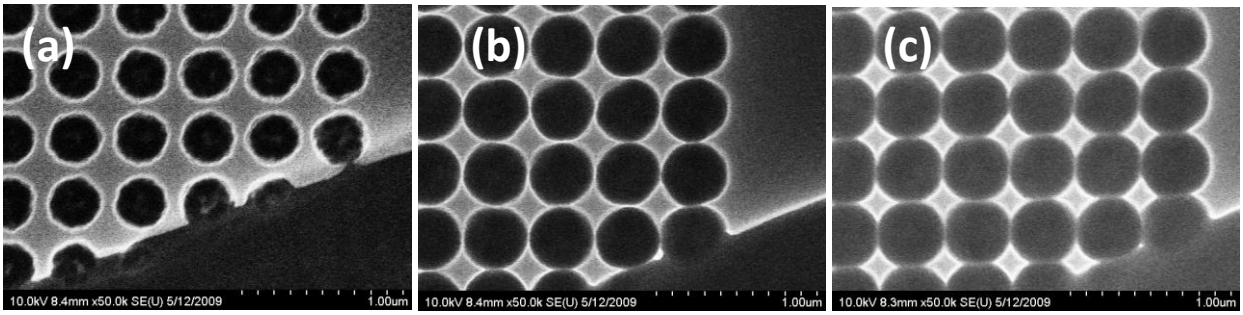


**Figure 10. (a) Silicon wafer without the isotropic etch. (b) Silicon wafer after a 2 minute etch. (c) Silicon wafer after a 4 minute etch.**

SOI wafer-1 was processed up to step 6 at UT Austin. It was subsequently etched with $SF_6$ at UTEP. $SF_6$ was required avoid etching the SilSpin mask while having a rapid silicon etch rate. Estimated etch rate was 35 nm/min in the lateral direction (x/y plane), and >60 nm/min in the vertical, z-direction. The parameters used for etching is shown in Table 2. Scanning Electron Microscope (SEM) images of the nanopatterned SOI wafer is shown in Figure 11. 40 nm diamond shaped silicon islands with extremely sharp features are clearly observed.

**Table 2. Etch parameters used on the SOI wafer.**

| Parameter | Value | units |
|---|---|---|
| Pressure | 0.025 | Torr |
| Power | 50 | Watts |
| Time | 3 | Minutes |
| $SF_6$ | 20 | Sccm |

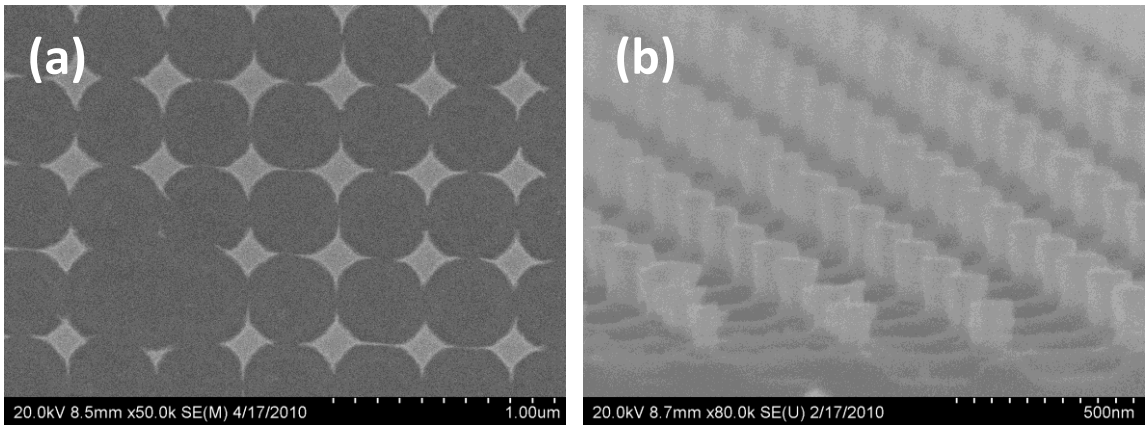


**Figure 11. (a) Top and (b) oblique view of a NIL pattern on SOI etched at UTEP.**

### *2.1.2 Micropatterning*

Micron scale patterning can be achieved with conventional photolithography. The photoresist thickness on the patterned samples was approximately 2 um as shown in Figure 12.

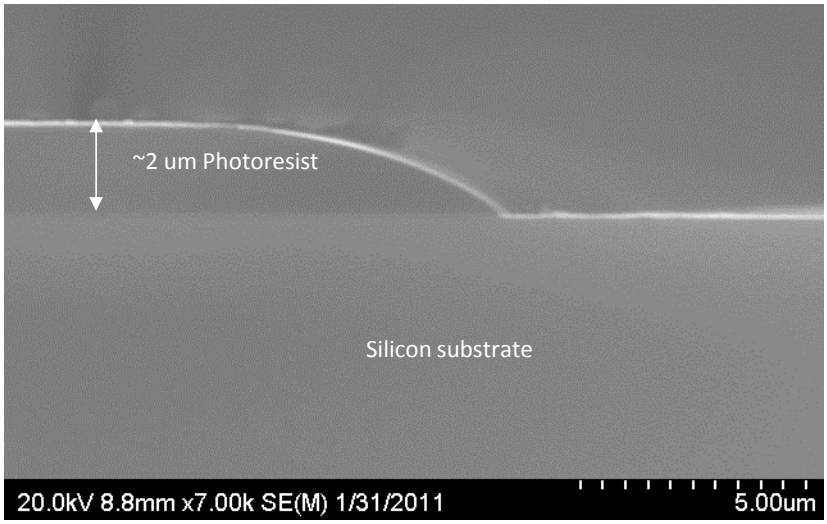


**Figure 12. Photoresist on a silicon substrate. Thickness ~2 um.**

Dry etching was used to transfer the photoresist pattern into the silicon wafer using $SF_6$. The parameters were tuned to achieve vertical sidewalls near the top of the pillars and are listed in Table 3. Process development was required to achieve vertical walls as illustrated in Figure 13. While it is possible that it could be further improved, these parameters were deemed adequate for the desired application. The final micro-patterned silicon wafer with photoresist removed is shown in Figure 14. Micrometer size pillars can be observed.

**Table 3. Etching parameter used for micropatterned silicon samples.**

| Parameter | Value | units |
|---|---|---|
| Pressure | 0.04 | Torr |
| Power | 200 | Watts |
| Time | 5 | Minutes |
| $SF_6$ | 15 | Sccm |
| Ar | 15 | Sccm |
| $O_2$ | 5 | sccm |

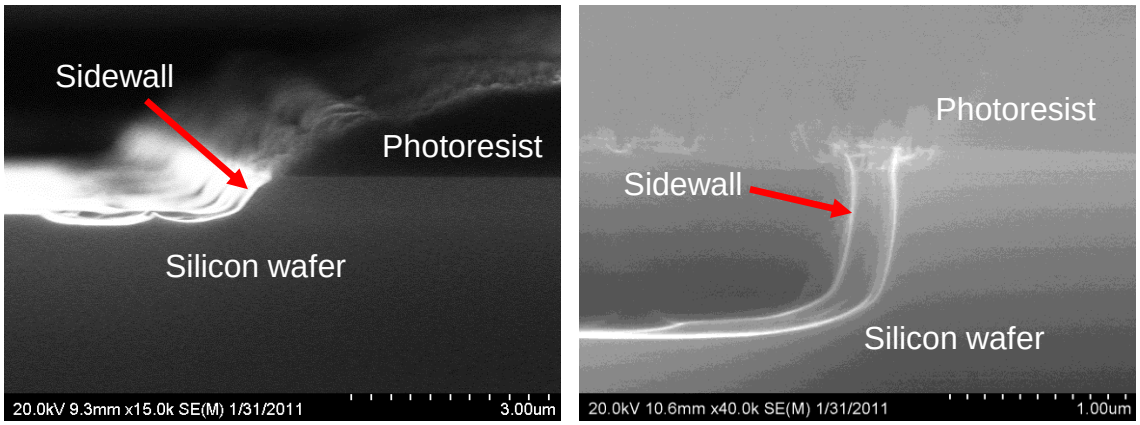


**Figure 13. Cross-sectional SEM images showing the silicon sidewall (a) before and (b) after etching process optimization to achieve vertical sidewalls.**

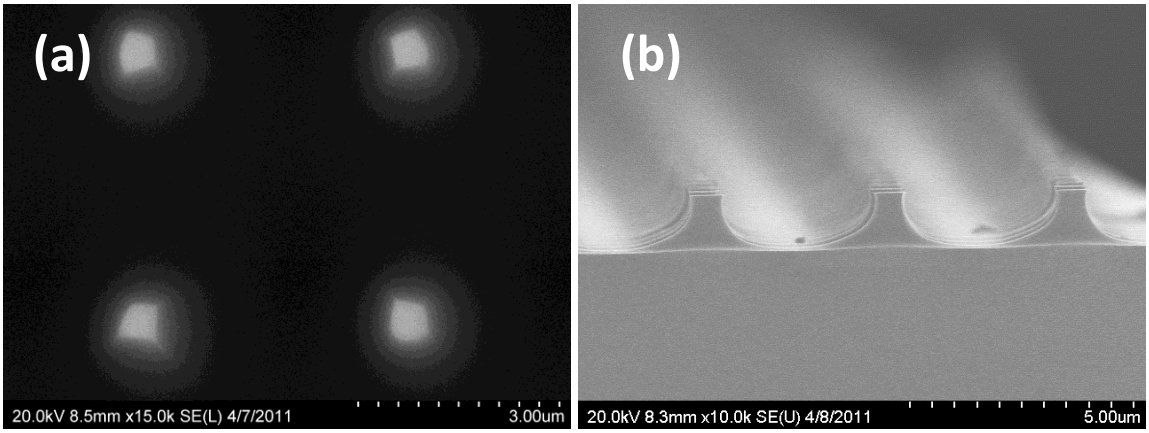


**Figure 14. (a) Top and (b) cross sectional views of a micropatterned sample.**

## 2.2 Sample Cleaning

As silicon reshaping is a primarily surface based phenomenon, the importance of a clean surface is critical. This includes the removal of the native oxide layer. When the RCA cleaning method is performed, the silicon surface but will contain a chemical oxide layer. Therefore, an oxide-etch step is performed with BOE immediately before heat-treating the samples. The surface will be clean of any native oxide and covered with a hydrogen terminating layer. This layer of hydrogen resists the formation of the native oxide on the silicon substrate and is ideal to ensure the cleanliness of the samples being annealed.

The complete cleaning procedure for the all the silicon samples used in the experiments is as follows:

**Cleaning of the beakers.** All the containers used to clean the sample are first cleaned themselves.

1. DI water rinse all beakers
2. A small amount of "piranha" (2 $H_2SO_4$:1 $H_2O_2$) is mixed in of the beakers
3. The piranha solution is divided into all the containers to be used
4. Each container is individually tilted and rotated to cover as much as the internal surfaces as possible with the solution.
5. The solution is discarded into a waste container.
6. DI water rinse all beakers
7. Nitrogen dry

**Cleaning of the samples.**

1. Soak in piranha solution for 5 minutes
2. Rinse in DI water
3. Etch in BOE for 1 minute
4. Rinse in DI water
5. Dry with Nitrogen

## 2.3 Annealing Experiments

The initial experiments were based on the assumption that the reshaping of the silicon nanostructures was due to a reduced melting point effect as reflected by the strategies used in their execution. Latter experiments focus instead on reshaping through hydrogen or argon annealing.

### *2.3.1 Annealing in a CVD Reactor – Preliminary Results*

Experiments performed by D. Zubia (unpublished) in the year 2000 exhibited what appeared to be reduced melting point for silicon nanostructures. In this case, the nanostructures were made by interferometric lithography and reactive ion etching on SOI wafers. Diagrams of the nanostructures are presented in Figure 15. The nanosized pillars have a diamond shape when seen from the top, with a diagonal length of between 80 and 300 nm and separated by 360 nm to 800 nm. The height of these nanostructures was 40 nm.

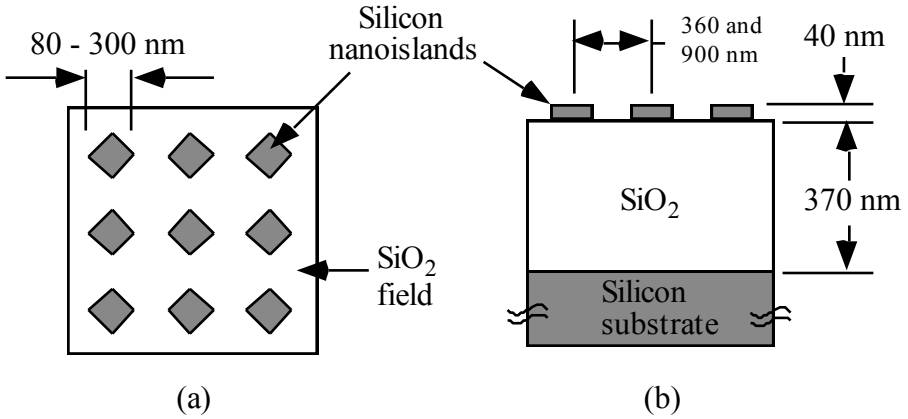


**Figure 15. Schematic (a) top and (b) cross sectional views of silicon nanostructures on SOI.**

### *Heating procedure*

The samples were cleaned using the following procedure:

**Table 4. Cleaning procedure for nanopatterned SOI samples.**

| Step # | Procedure |
|---|---|
| 1 | Ultrasonic soak in trichloroethylene for 5 minutes |
| 2 | Ultrasonic soak in acetone for 5 minutes |
| 3 | Soak in isopropyl alcohol for 1 minute |
| 4 | Rinse with de-ionized water for 5 minutes |
| 5 | Soak in fresh "piranha" (5 $H_2SO_4$:1 $H_2O_2$) for 5 minutes |
| 6 | Rinse with de-ionized water for 5 minutes |
| 7 | Dry with nitrogen |
| 8 | Etch in BOE (3[7$NH_4F$:1HF]:1$NH_4OH$) for 3-12 seconds |
| 9 | Rinse with de-ionized water for 5 minutes |
| 10 | Dry with nitrogen |

The samples were placed in an MOCVD chamber immediately after cleaning. The temperature profile used for these experiments is shown in Figure 16. The samples were heated at several temperatures ranging from 880 °C to 1105 °C for 5 minutes at 100 Torr.

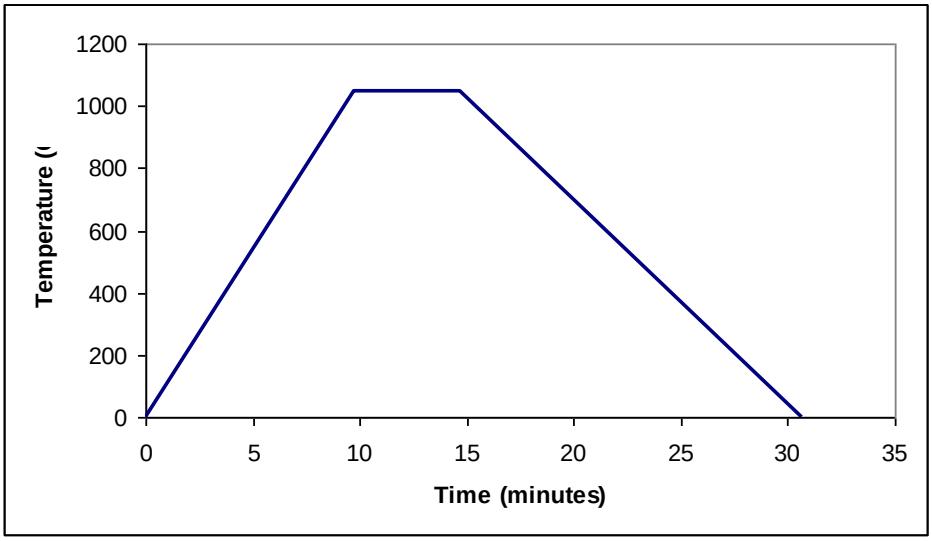


**Figure 16. Temperature profile for samples annealed in hydrogen for 5 minutes.**

### *Results*

The samples annealed by this method presented clear reshaping when the temperature exceeded 1030 °C. No reshaping was observed in samples annealed at under 1000 °C. **Error! Reference source not found.** shows samples annealed at various temperatures.

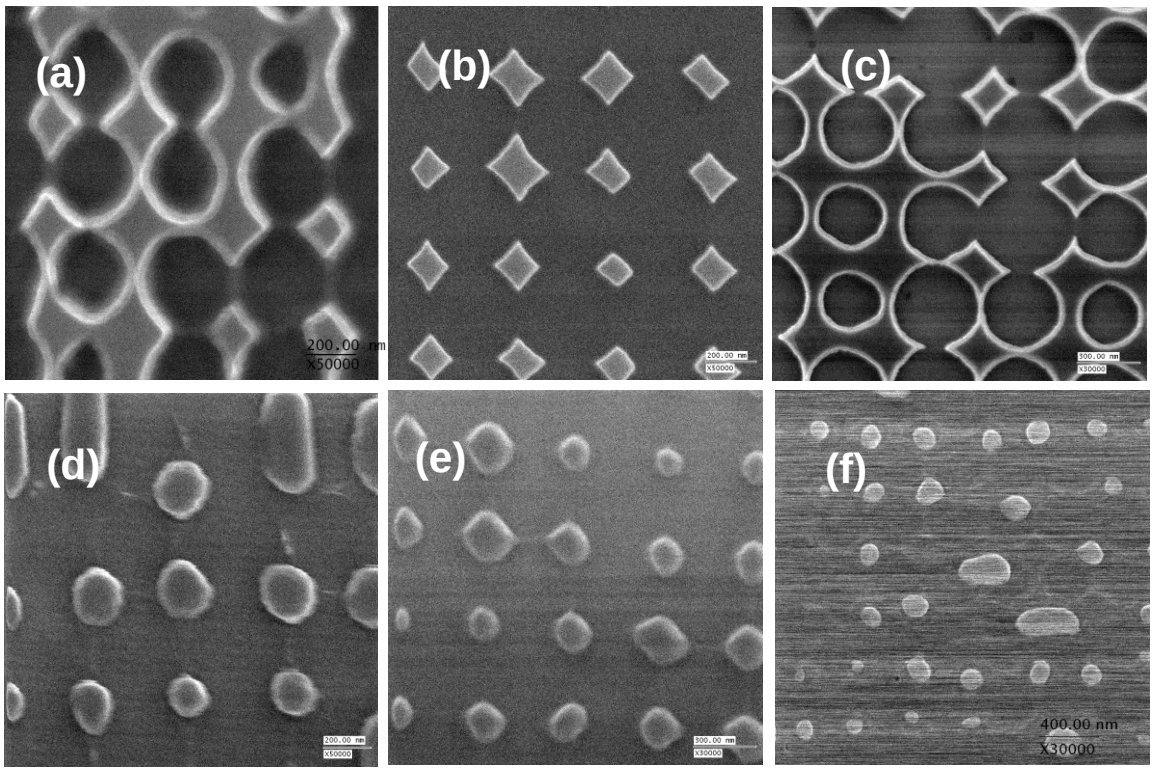


**Figure 17. Samples annealed in a MOCVD chamber under a 100 Torr Hydrogen atmosphere at (a) 880 °C, (b) 940 °C, (c) 1000 °C, (d) 1030 °C, (e) 1060 °C, and (f) 1105 °C.**

As observed in Figure 17, the reshaping of the silicon nanoislands does not occur for the samples annealed at or under 1000 °C, while significant reshaping happened for all the samples annealed at or over 1030 °C. This sharp difference indicates the existence of a transition temperature at which reshaping takes place. Because of this sharp transition, the explanation that best fits this data is a reduced melting point effect. Melting is a phenomenon that occurs within a very narrow temperature window. After melting, the shape would be dictated by surface tension causing rounding of the rounding of nanoislands.

### *2.3.2 Annealing in a Box Furnace*

The first set of experiments performed at UTEP was done on a SentroTech ST-1600C-445 box furnace (Figure 18). This box furnace has a gas inlet port for nitrogen or argon, a temperature ramp rate of 10 °C/min, and a maximum temperature of 1600 °C. It is important to note that this furnace is not hermetic, and while the gas inlet can be used to minimize the atmospheric contamination, the annealing atmosphere will still contain some percentage of the gasses that form the normal part of the atmosphere.

The objective of this set of experiments was to replicate the result from the preliminary experiments assuming this result was due to a reduced melting point effect. Therefore, nanotextured samples were used for this set of experiments.


**Figure 18. SentroTech ST-1600C-445 box furnace.**

***Procedure***

1. The samples were imaged using a Hitachi S-4800 Scanning Electron Microscope (SEM).
2. The samples were cleaned as discussed in section 3.2 and placed into the box furnace within 5 minutes of cleaning. The samples were placed on top of an alumina crucible

3. Nitrogen was flowed into the furnace at 100 sccm for 30 minutes without any heating.
4. The temperature ramp was set and initiated after purging the furnace. The temperature profile is illustrated in Figure 19.
5. Once the furnace had cooled, the sample was removed and imaged again with the SEM to try to observe the reduced melting point effect.

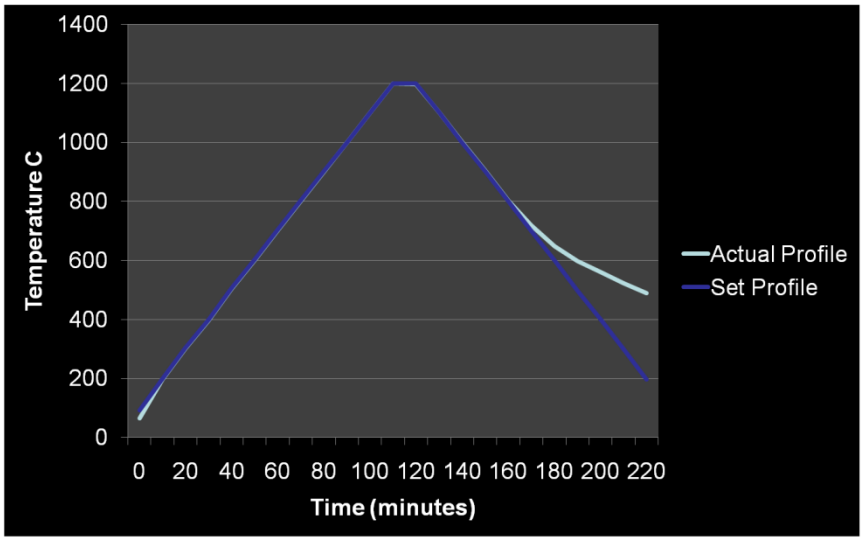


**Figure 19. Temperature profile for samples placed in the SentroTech box furnace.**

The temperature profile was varied for the different experiments. The ramp rate was held constant, the dwell temperature was varied between 1000 and 1300 °C, and the dwell time was varied between 10 and 60 minutes.

### *Results and analysis*

Figure 20 illustrates the surface morphology of one sample heated to 1200 °C and annealed for 10 minutes. Rounding of the corners is evident. However, for this and other samples, ellipsometry and cross section imaging of the samples revealed the presence of an oxide between 30 and 300 nm in thickness. As the objective of these experiments was to open the path for direct silicon to silicon bonding, silicon oxide is unacceptable. Dramatically increasing the nitrogen flow to purge the chamber was not sufficient to eliminate the oxidation problem. Figure 21 shows a cross section of an annealed silicon sample on which significant oxide was grown. It was concluded that a different heating apparatus would be required for the successful reshaping of silicon.

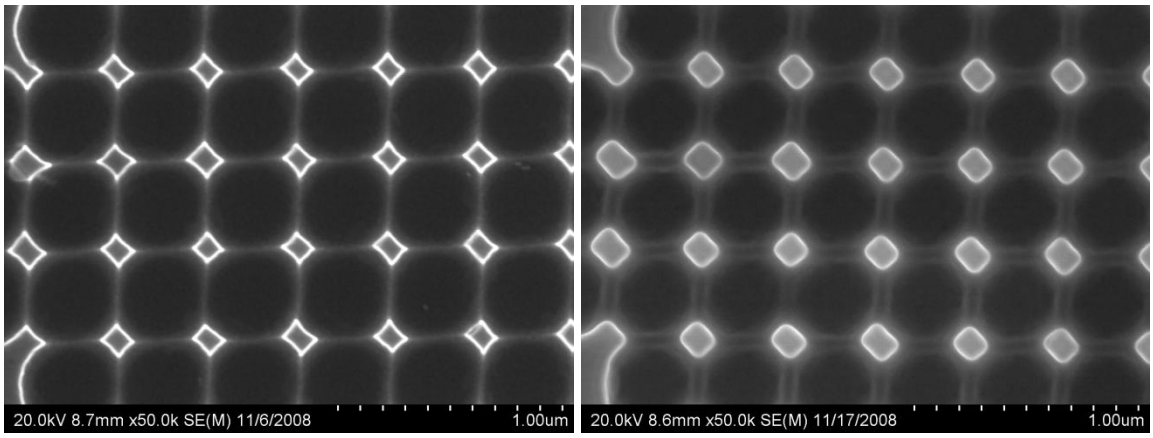


(a) (b)

**Figure 20. A nanopatterned sample (a) before annealing and (b) after a 10 minute anneal at 1200 °C. Significant reshaping due to oxidation is observed.**

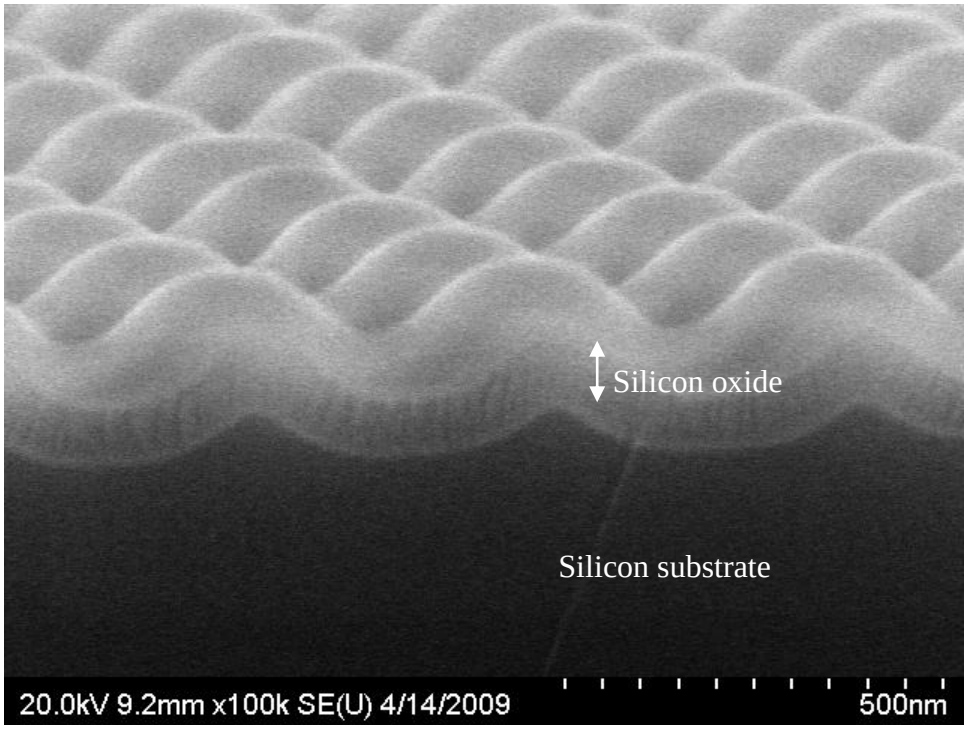


**Figure 21. Oxidation visible on the cross section of a cleaved sample after annealing.**

### *Other Observations*

Imaging of the samples had an effect on the oxide growth as illustrated in Figure 22. While no further experimentation was conducted on the issue, it is likely that the origin of this phenomenon is the charges trapped in the native oxide after the initial imaging. Charge buildup can be observed in the SEM as areas that appear darker than their surroundings and often occurs when a long time is spent imaging an area. These charges may have remained after the chemical cleaning and locally changed the oxidation rate.

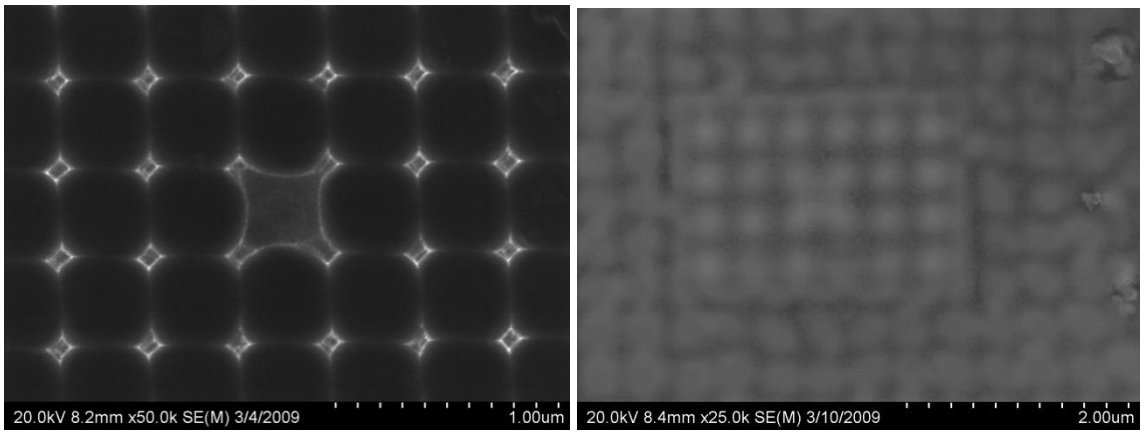


**Figure 22. Different oxidation rate at the point where the silicon had been imaged for a long time, causing charge buildup in the native oxide.**

### *2.3.3 Annealing in a Quartz Tube Furnace*

The second set of experiments was performed in Thermtec Quartz tube furnace (Figure 23). This tube furnace has two gas inlets, which allow the use of gas mixtures; a temperature ramp rate of 25 °C/min; three semi separate heating zones; and a maximum temperature of 1150 °C. While this tube furnace was not hermetically sealed either, the tube setup is much more effective for purging with an inert gas. Pressure cannot be controlled and only atmospheric pressure can be used.

This set of experiments also focused on trying to observe a reduced melting point effect and used nanotextured silicon samples. Nitrogen was the primary annealing atmosphere; hydrogen and argon were used in limited amounts.


**Figure 23. Thermtec tube furnace.**

***Procedure Used***

**Cleaning**

1. Piranha – 5 minutes
   - 1 $H_2O_2$ : 2 $H_2SO_4$
2. BOE – 1 minute
   - 3 BOE : 1 $NH_4OH$

The cleaning is done both on the sample and on the wafer used to hold the sample while in the furnace. The quartz boat was cleaned with DI water only and dried with $N_2$.

**Heating procedure**:

1. Sample placed in the furnace immediately after cleaning (2 minutes)
   - Boat placed in the middle of the furnace according to a predetermined marker on the pushing rod.
   - Quartz tube is closed with the cap which has a hole for ventilation. Hole points towards the vent tube
   - This in turn is covered with an aluminum sheet to minimize air flow.
2. $N_2$ flow turned on
   - UHP $N_2$ flows into the furnace for 15 minutes before turning it on.
   - Flow set at 90 sccm.
3. Furnace temperature is set and turned on.
   - Left zone temperature offset: +10 C
   - Center zone temperature: 1150 C
   - Right zone temperature offset: +10 C
4. Furnace temperature is lowered (Heating off)
   - Done ½ hour after the center zone reaches the set temperature value. 1hr 50min after turning on the furnace is the standard for 1150 C.
   - Left: -99 ; Center: 0 ; Right: -99
   - When temperature reaches 150 C the nitrogen flow is closed.
   - The temperature profile is illustrated in Figure 24
5. Sample is removed from the furnace when temperature reaches ~60 C

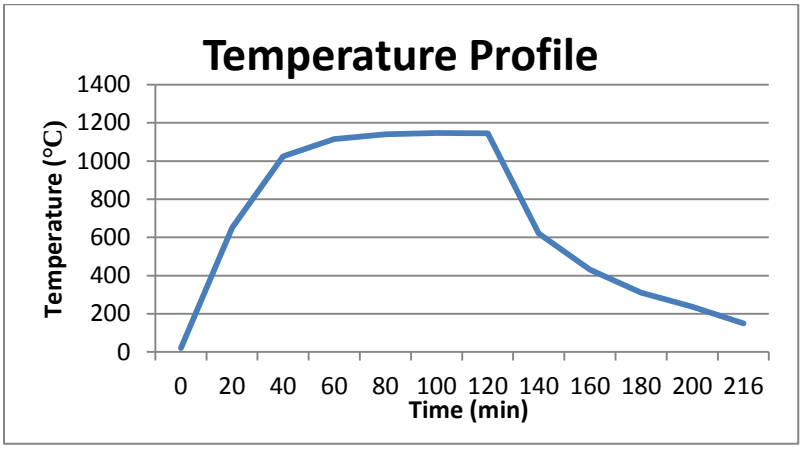


**Figure 24. Temperature profile for samples placed in the THERMTEC tube furnace.**

Hydrogen was also used in some of the experiments from forming gas. Forming gas is a mixture of at least 90% nitrogen and 10% hydrogen. Hydrogen diluted in this manner is below the ignition level and therefore safe to use in an open furnace. Regardless, the forming gas was further diluted using ultra high purity (UHP) nitrogen to achieve an atmosphere of 95% nitrogen and 5% hydrogen. Pure argon was also used as annealing atmosphere. The temperature profile was not varied.

### *Results and Analysis*

The experiments were performed in three atmospheres: Nitrogen, forming gas, and argon.
The experiments in **nitrogen** were largely succesful in avoiding oxidation. The oxide was measured at as low as 1 nm with ellipsometry, showing a 99.98% goodness of fit. 1 nm is close to the experimentally measured native oxide in silicon. However, the samples did not exhibit any change in surface morphology, as illustrated in Figure 25.

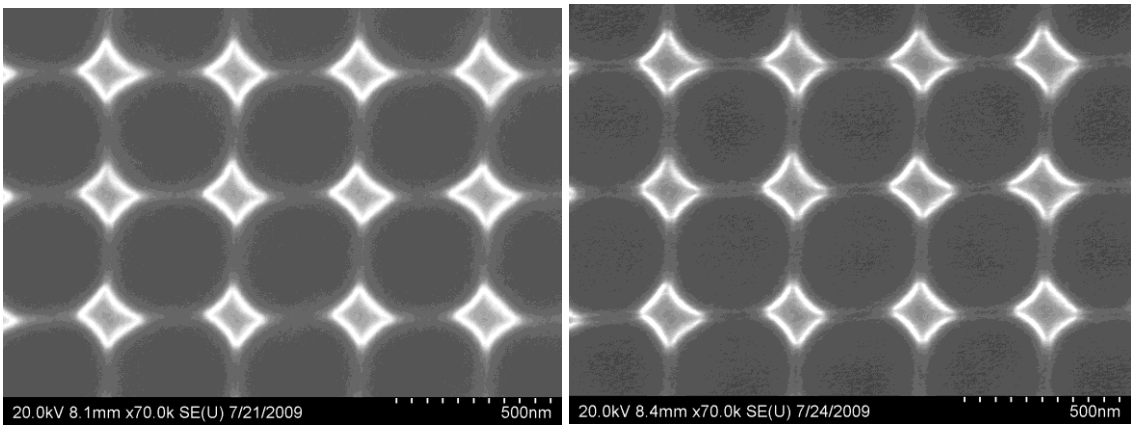


(a) (b)

**Figure 25. Silicon sample (a) before and (b) after annealing at1150 °C in nitrogen.**

The conclusion from these experiments was that nitrogen may not be a sufficiently clean atmosphere. Given that the reduced melting point depends on surface effects, even a native oxide may be enough to supress it. In the context of hydrogen/inert atmosphere reshaping, nitrogen has been shown to block the reshaping effect, which is consistent with these results.

In an effort to further reduce the possibility of an oxide forming on the surface of the silicon sample, **hydrogen** was introduced in the form of Forming gas. To ensure the safety in the execution, the hydrogen level was monitored using a HY Alerta 500 handheld hydrogen leak detector from H2SCAN. The hydrogen levels were primarily monitored at the exhaust port of the tube furnace. For safety, other points of interest were also monitored such as the roof and the gas inlet ports. The result of the forming gas annealing is presented in Figure 26.

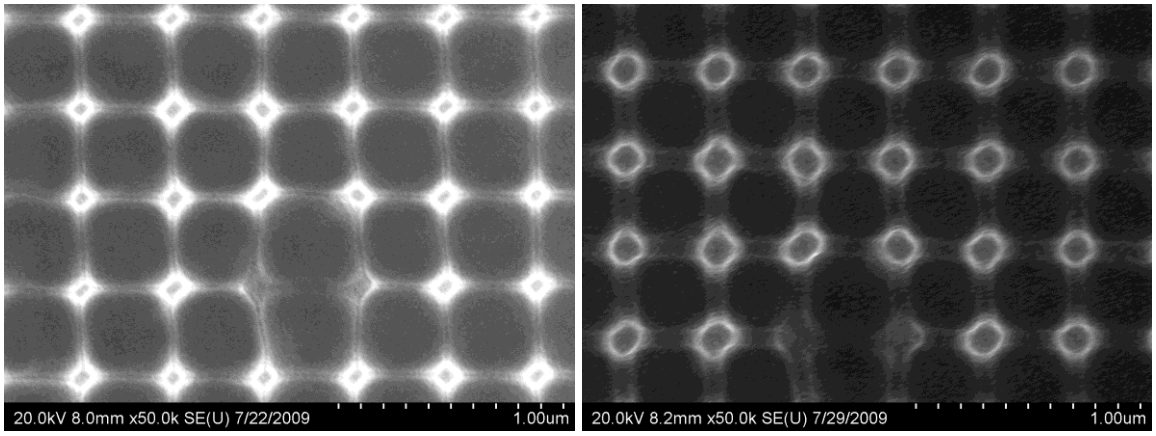


(a) (b)

**Figure 26. Silicon sample (a) before and (b) after annealing at1150 °C in forming gas.**

All the forming gas annealed samples showed oxide layers of ~30 nm, even when increasing the gas flow. This suggests that the reason for the oxidation is not oxygen coming into the tube from the exhaust.

Contrary to the expectations, the hydrogen level at the exhaust did not stay constant, instead it decreased with increasing temperature and dropped below the lower detection limit before reaching the annealing temperature. This means that the hydrogen was being consumed before leaving the tube. The reaction that consumed the hydrogen was probably between the silicon oxide from the quartz and the hydrogen gas, generating water vapor that is not detected by the HY Alerta. This water vapor is in turn the likely reason for the increased oxidation of the silicon samples.

It was concluded therefore that while forming gas may normally help in the reshaping by minimizing oxidation, it cannot be used in conjunction of a quartz tube because the tube is a source of oxigen which affects the outcome of the experiment.

As an alternative inert atmosphere, **argon** was used to anneal the samples. The flow level used for argon was the same as the one used for nitrogen with the single intention of impeding oxidation. The results from this test are presented in Figure 27. While there is evidence for some reshaping, a much more prevalent effect was the thermal etching of silicon, consistent with the available literature.

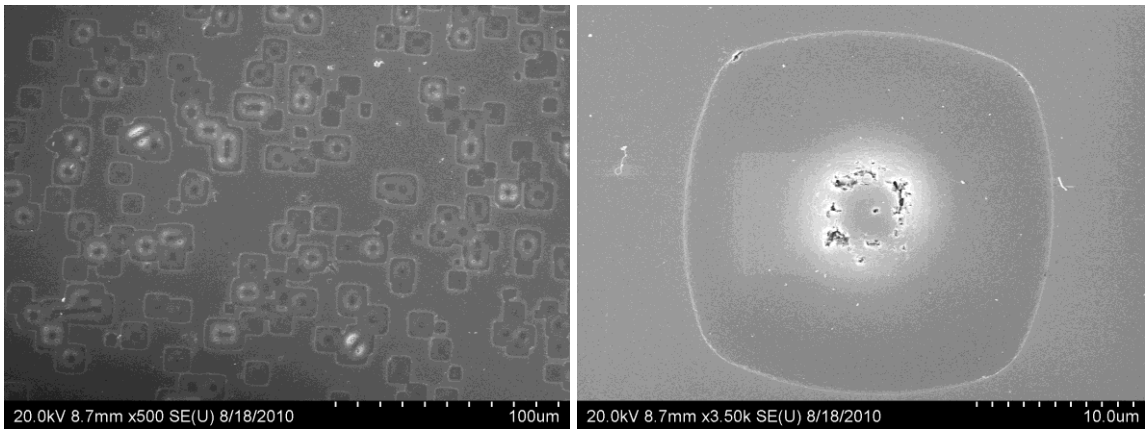


**Figure 27. Thermal etching damage on the silicon surface.**

Some reshaping might have occurred, however the thermal etching was deemed too extensive to be acceptable, leaving the annealed samples unusable. The amount of etching is illustrated in Figure 28 while a cross section of an annealed sample is presented in Figure 29. In the presented cross section, some amount of rounding has taken place, as the top surface of the pillars is no longer flat.

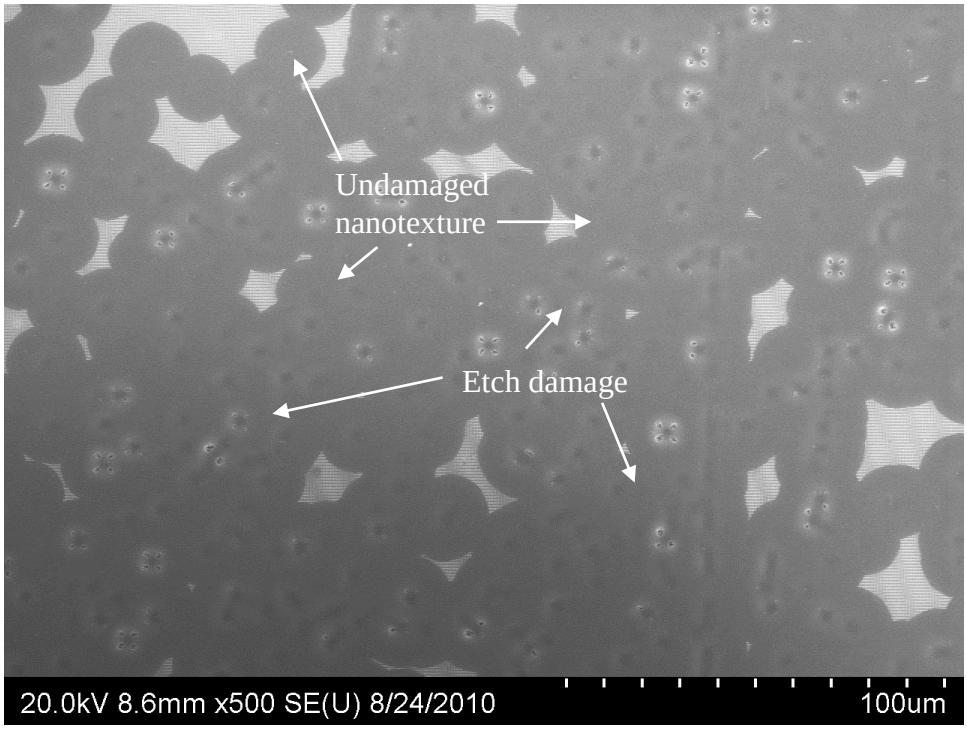


**Figure 28. Etching damage on a nanotextured Si sample. The pattern remains only on the brighter areas of the image.**

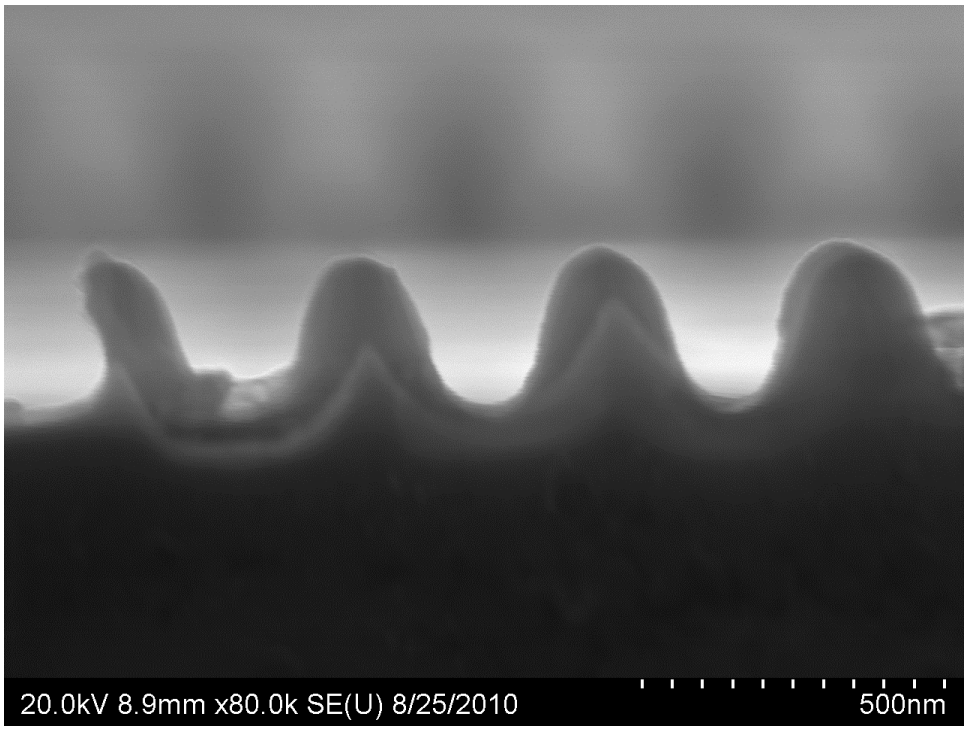


**Figure 29. Silicon nanopillars where the flat top has been moderatelly rounded. The leftmost pillar has been damaged by thermal etching.**

Samples annealed in argon did not exhibit significant oxidation, as observed from cross sectional SEM imaging. Due to the much more increaed surface roughness, reflectometry measurements could not provide any oxide thickness information.

The final conclusion from the annealing experiments performed in the quartz tube furnace was therefore that impurities in the atmosphere arising from both the tube, and from gasses not properly purged were impeding the reduced melting point effect from taking place. To adress this problem, annealing in a different apparatus is required. In the context of reshaping through hydrogen annealing, nitrogen has been shown to block the reshaping effect with or without the presence of a surface native oxide. This remains true for mixtures of hydrogen and nitrogen, even when no oxidation occurs. Argon has been demonstrated to be a working annealing atmosphere, however etching present here and in published experiments has kept it from gaining more appeal.

### *Other Observations*

An interesting finding is that nanowires of unknown origin and composition spontanously formed on top of the silicon samples annealed in a forming gas atmosphere. A possible explanation of the nature of these nanowires is that they self assemble out of the silicon left from the quartz after the hydrogen from the forming gas has removed the oxigen, as reported by M.W. Shao who performed a similar experiment. These nanowires are shown on Figure 30.

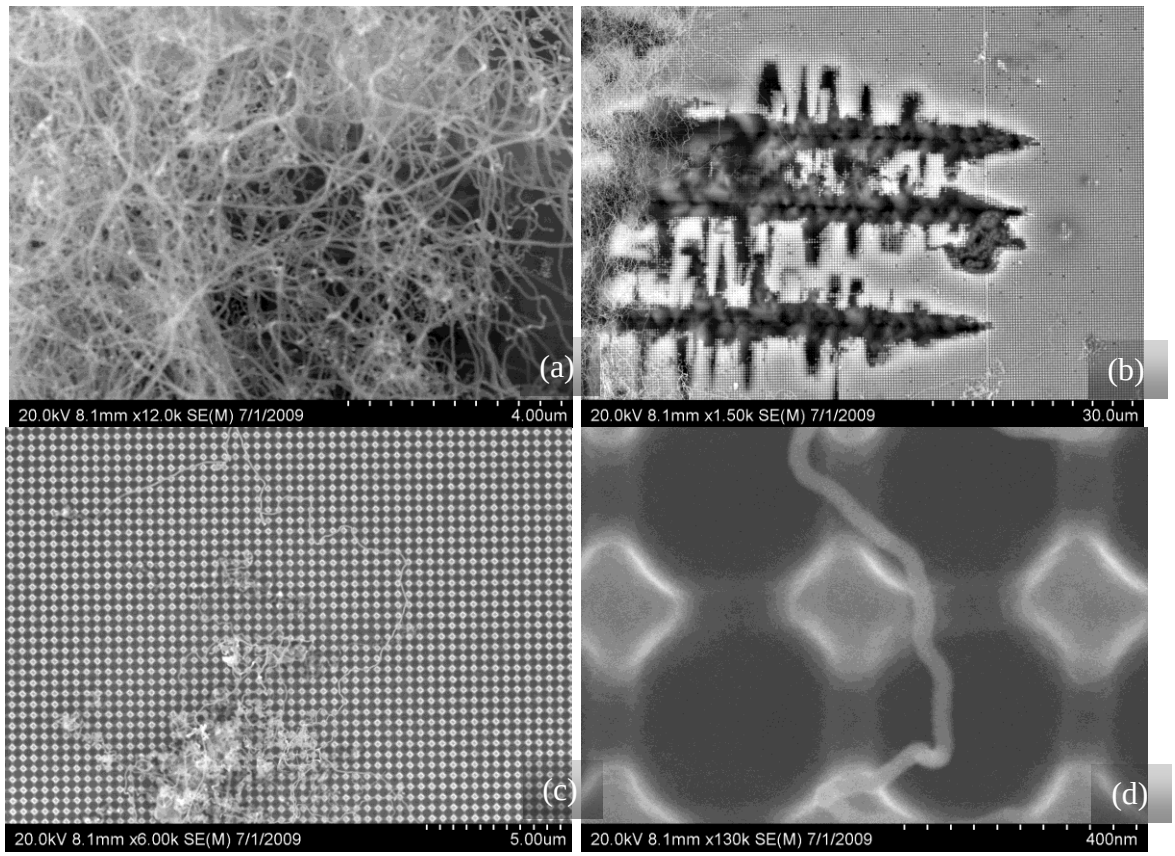


**Figure 30. Self assembled nanowires on the patterned silicon surface showing: (a) a high density nanowire cluster; (b) nanowire group next to etch damage on the silicon; (c) a few nanowires on a patterned surface; and (d) a single nanowire on top of the diamond structures.**

### *2.3.4 Annealing in a High Temperature XRD Stage*

The following set of experiments was conducted in a berillyum high temperature stage on an X-Ray diffraction machine. This is an all metal high temperature stage equipped with a platinum heating strip. It is equiped with a turbomolecular pump for evacuation to high vacuum, capable of achieving a base pressure of $10^{-6}$ Torr. No gas inlet is available, therefore vacuum is the only annealing atmosphere possible. The maximum temperature of this stage is 1400 °C. The X-ray diffractometer and high temperature stage are illustrated in Figure 31 and Figure 32.

The objective of these experiments remained to observe the reduced melting point of silicon nanoislands. Unfortunatelly the sample is normally placed directly on the platinum heating strip, and because silicon reacts with platinum when the temperature exceed 900 °C, an intermediate ceramic holder was used. Two types of ceramic were used: a 1 inch by 1 inch high purity alumina sheet of 0.5 mm thickness, and a section of a sapphire wafer.

**Figure 31. Discover D8 X-Ray Diffractometer from Bruker**

**Figure 32. High temperature heating stage mounted on the X-ray diffraction equipment.**

### *Procedure Used*

As much as possible, contamination was removed by chemical cleaning before annealing the sample. Most of the stage was assembled in the X-Ray diffractometer before performing the cleaning to minimize the time the sample spent exposed to the atmosphere after cleaning and before annealing.

**Heating stage cleaning.** The heating stage was cleaned first and then assembled on the diffractometer. Once assembled it was vacuumed out to keep the contaminants out. Assembly took approximately 10 minutes. It was cleaned using a lint free cloth moistened with the following chemicals:

1. Acetone
2. Methanol
3. DI water
4. Nitrogen Dry

**Ceramic cleaning.** The ceramics were cleaned next using regular solvents to minimize contamination. After cleaning the piece to be used, it was placed inside a non-hermetic acrylic box where it remained for approximately 30 minutes before being transferred to the heating stage. Cleaning steps:

1. Acetone – 5 minutes
2. Methanol – 5 minutes
3. DI water rinse – 5 minutes
4. Nitrogen Dry

**Sample cleaning.** The sample was cleaned as per the regular procedure in clean beakers and then transferred to a non-hermetic acrylic box where it remained for approximately 10 minutes before being transferred to the heating stage

1. Piranha – 5 minutes
   - 1 $H_2O_2$ : 2 $H_2SO_4$
2. DI water rinse
3. BOE – 1 minute
4. DI water rinse
5. Nitrogen dry

**Heating procedure**:

1. Sample placed in the furnace as soon as possible after cleaning
   - Ceramic used centered on top of the platinum heating strip.
   - Heating stage is closed with the beryllium dome and tightened with the provided screws
2. Rough vacuum pump is turned on
   - Rough vacuum achieves a pressure of $10^{-2}$ Torr within 15 minutes of initiating the process.
3. Turbo molecular pump is turned on.
   - Turbopump reaches $10^{-6}$ Torr within ½ an hour of being turned on
4. Heating stage temperature profile is set determined and turned on.
   - Approximately 5 °C/min ramp rate
   - Target temperatures between 1000 and 1300 °C
   - Dwell time of 30 minutes.
   - Grazing incidence scans done every 100 °C at lower temperatures, and every 50 °C at higher temperatures.
5. Sample is removed from the furnace when temperature reaches ~60 C

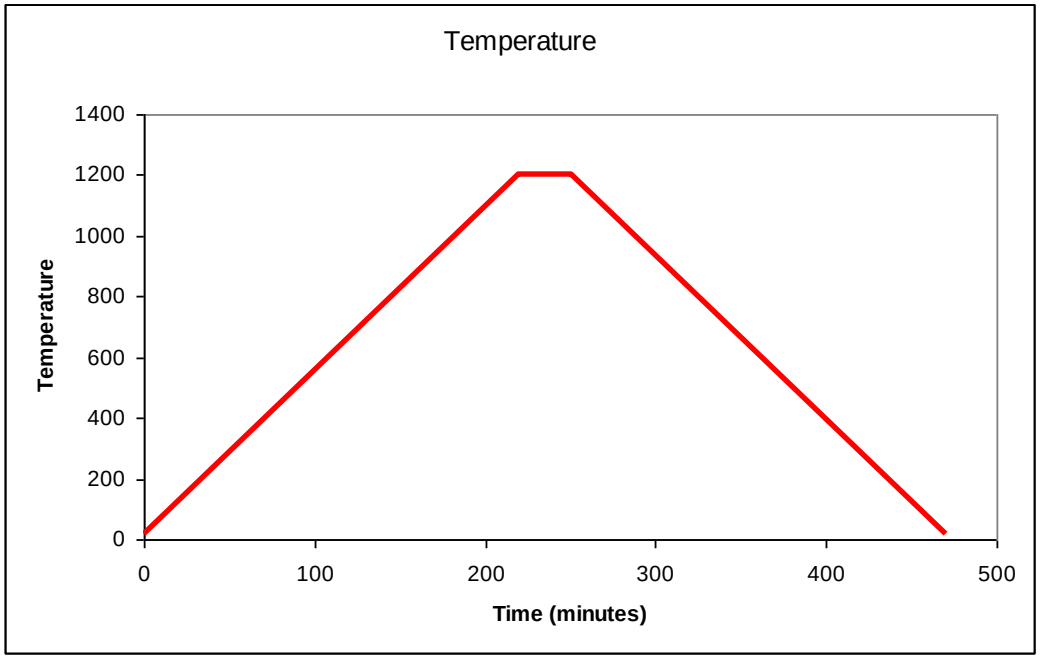


**Figure 33. The temperature profile for this heating method follows very closely the set point.**

### *Results and Analysis*

The two main problems from the previous heating experiments were eliminated by using the all metal high temperature stage. No oxidation could be detected through either ellipsometry, or by observing the cross section in the SEM. However, no reshaping took place either at the experiments that were completed up to 1200 °C. No results could be reported for higher temperatures because of problems with the holding ceramics used. Figure 34 illustrates the results of annealing in this high temperature stage.

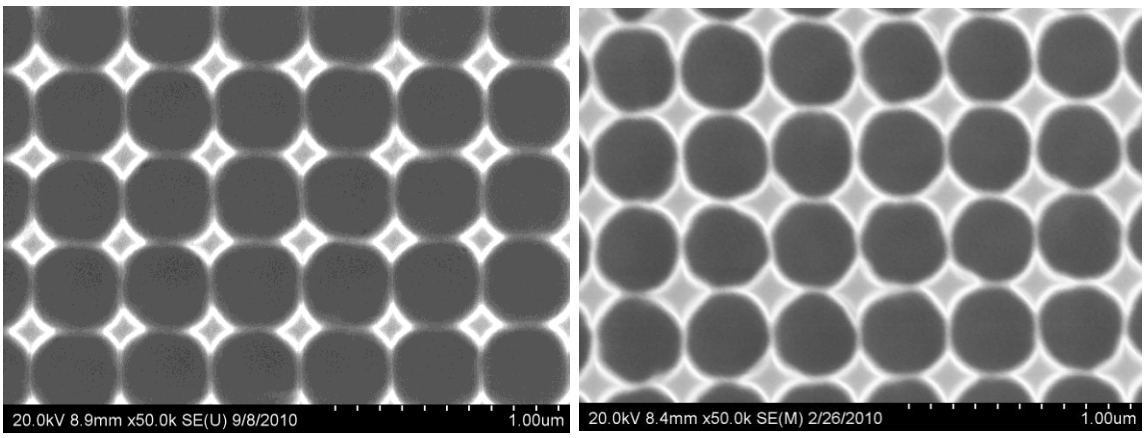


(a) (b)

**Figure 34. Silicon nanotexture (a) before and (b) after annealing in high vacuum for 30 minutes at 1200 °C. Different sections of the sample were imaged but annealing did not cause any corner rounding.**

No oxidation, no etching and no change is observed in these samples. The intermediate layer was at first blamed as being a source of interference by thermally insulating the sample from the heater. However an accident that occurred during the heating for one particular experiment proved this argument wrong. For the results presented in Figure 34, the holding ceramic broke when the temperature was > 1200 °C. The sample fell on the platinum heater exposing the silicon directly to the high temperature and causing a small amount of alloying at the bottom of the sample to form where it was in contact with the platinum strip. On the top patterned side of the sample, nevertheless, there was still no reshaping even when exposed directly to this temperature.

This result forced a reevaluation of the initial assumptions of a reduced melting point effect at the scale at which these samples were patterned, which eventually led to the findings of T. Sato and other authors who explain the reshaping effect as being due to hydrogen exposure. In the context of atmosphere reshaping, some reshaping has been demonstrated under ultra high vacuum conditions, but none at the vacuum range that these experiments were performed.

### *3.3.5 Annealing in an Alumina Tube Furnace*

To address the need for a hydrogen atmosphere, a tube furnace was selected which included vacuum flanges. A MTI GSL-1500X-40 tube furnace was used for this purpose. The equipment setup and design considerations are addressed in section 3.4. The vacuum level achievable in this setup is of 20 mTorr, controllable up to 400 Torr with a nitrogen flow, and up to 10 Torr with hydrogen flow. The tube material was initially Alumina. Another tube material used is the high temperature super alloy RA-330. The maximum temperature with the Alumina tube is 1500 °C but the maximum ramp rate is of 5 °C/min. For the superalloy tube the maximum temperature is 1200 °C and the ramp rate possible is greater than 100 °C/minute.

The objective of these experiments was to observe the reshaping through hydrogen annealing of silicon surfaces. Initial experiments were conducted using clean, non patterned silicon samples to observe the potential contaminants existent in this setup.

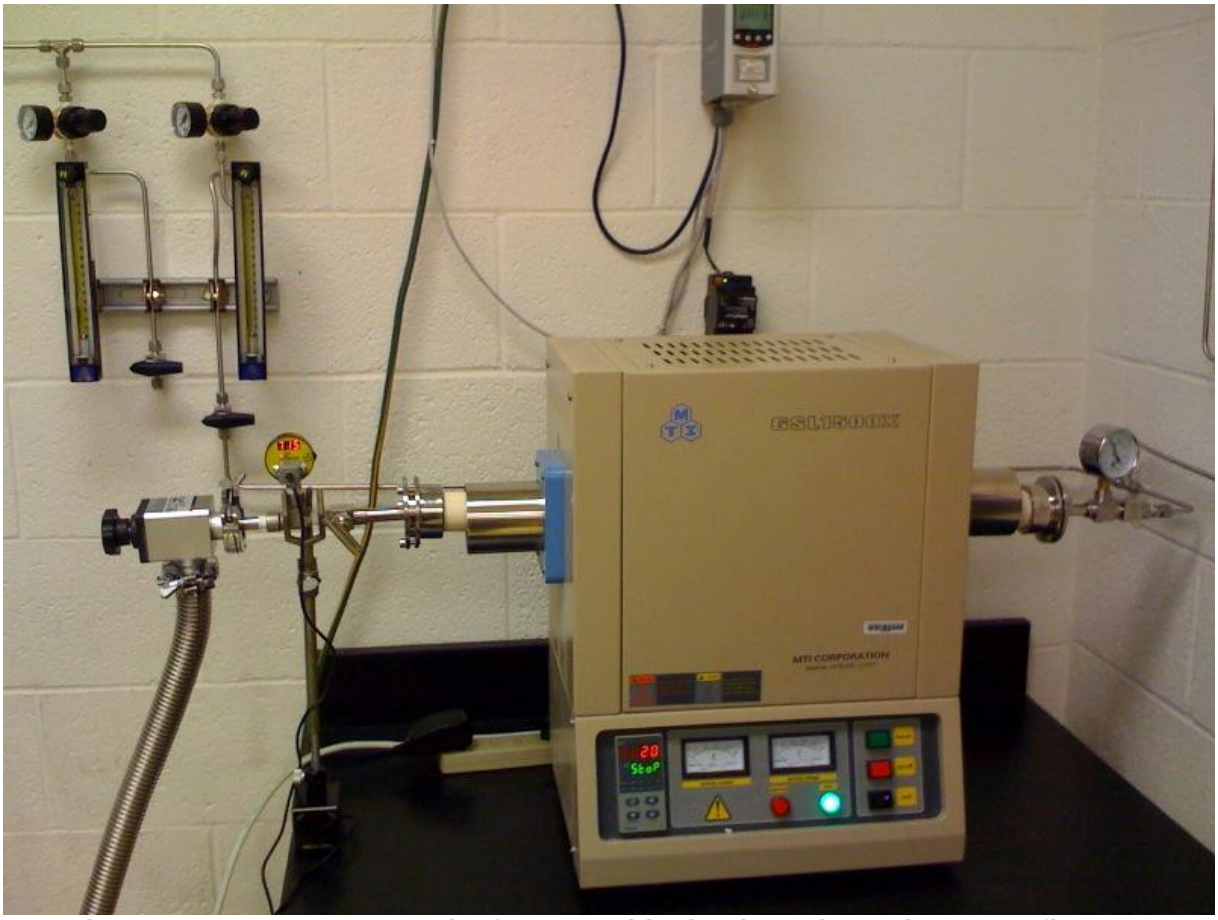


**Figure 35. GSL-1500X-40 tube furnace with alumina tube and vacuum flanges.**

### *Procedure Used*

Both the sample and the piece of alumina used to hold the sample were cleaned for these experiments, but neither the tube nor the alumina foam pieces used as part of this setup could be cleaned. The foam pieces were kept inside the tube and the tube was vacuumed out when not in use to minimize contamination. The same observation is made regarding the use of the RA330 super alloy.

**Holder cleaning.** The holder (alumina/RA330) was cleaned first using regular solvents to minimize contamination. After cleaning the piece to be used, it was placed inside a non-hermetic acrylic box where it remained for approximately 20 minutes before being transferred to the tube furnace. Cleaning steps:

1. Acetone – 5 minutes
2. Methanol – 5 minutes
3. DI water rinse – 5 minutes
4. Nitrogen Dry

**Sample cleaning.** The sample was cleaned as per the regular procedure in clean beakers and then transferred to a non-hermetic acrylic box where it remained for approximately 2 minutes before being inserted in the tube furnace.

1. Piranha – 5 minutes
   - 1 $H_2O_2$ : 2 $H_2SO_4$
2. DI water rinse
3. BOE – 1 minute
4. DI water rinse
5. Nitrogen dry

**Heating procedure**:

1. Sample placed in the furnace immediately after cleaning (2 minutes)
   - Holder with sample placed in the middle of the furnace according to a predetermined marker on the pushing rod.
   - One alumina/RA330 tube block is moved into position to protect the hermetic seals from radiant heat.
   - The tube is closed with the vacuum flange
2. Vacuum pump is turned on and the tube is purged with $N_2$
   - UHP N2 flows into the furnace for 30 minutes before turning it on.
   - Flow set at 4 slpm.
3. Furnace temperature profile is set and turned on.
   - Annealing atmosphere is changed to the desired conditions
   - Ramp rate: 5 °C/min (Alumina), 100 °C/min (RA330)
   - Target temperature between 1000 and 1300 °C (RA330 1200 °C)
   - Dwell time between ½ and 1 hour
   - The temperature profile is illustrated in Figure 36 (Alumina tube) and Figure 37 (RA330 tube)
4. Sample is removed from the furnace when temperature reaches ~60 C

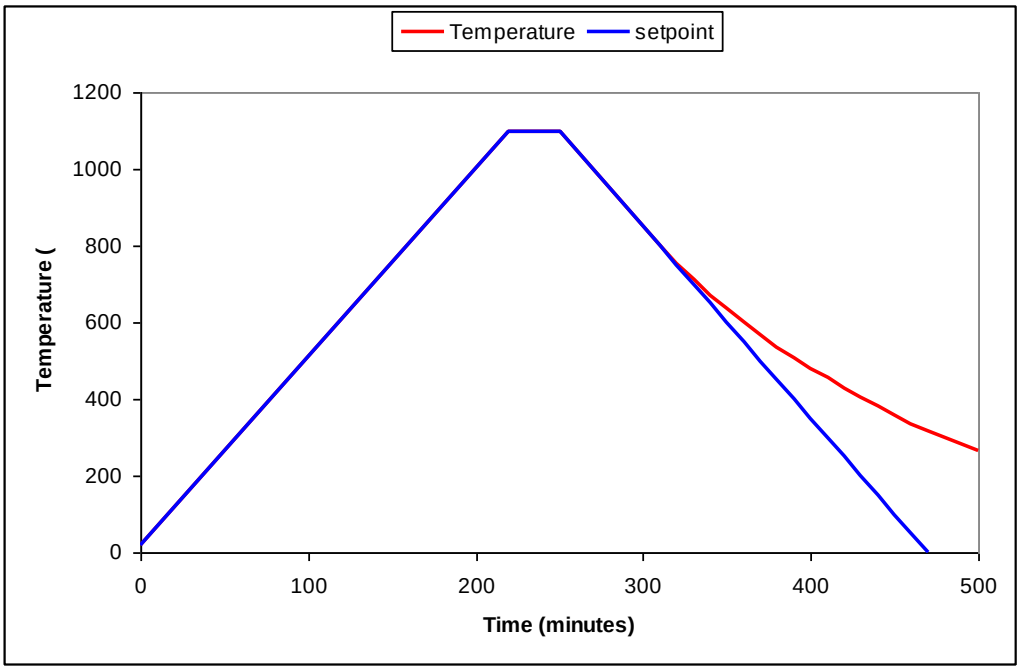


**Figure 36. Temperature profile for the Alumina tube.**

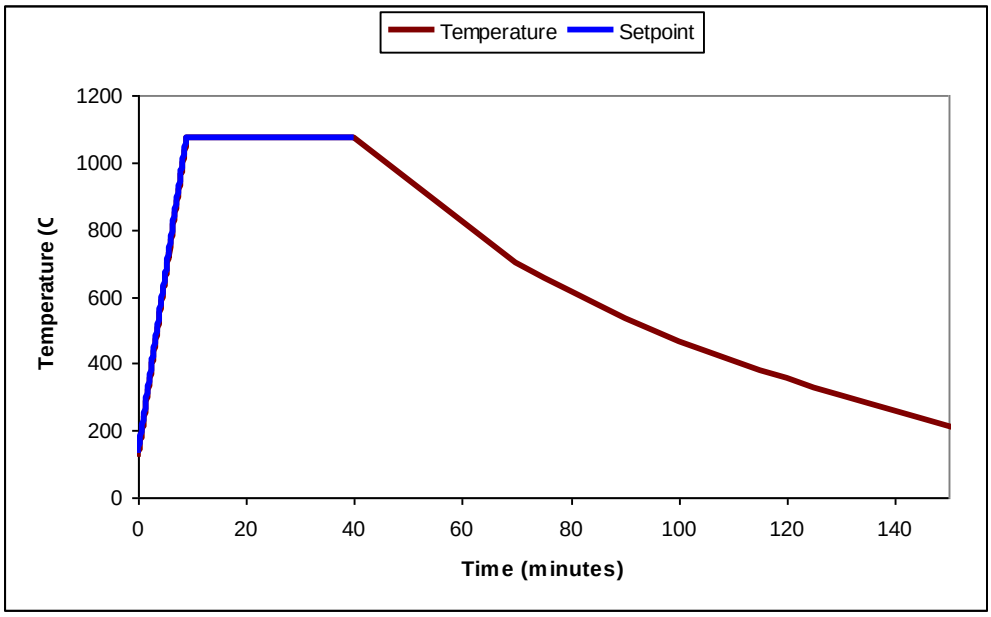


**Figure 37. Temperature profile for samples annealed in the RA330 tube.**

### *Results and Analysis*

Unfortunately, this setup brought back some of the issues that were the reason for other setups to be discarded. The alumina tube suffered from the same issues as the quartz tube. Namely, it became a source of oxigen and the very low ramp rate allowed significant etching to take place. To amplify and observe correctly these issues, a silicon sample was annealed at 1300 °C in a 5 torr nitrogen atmosphere for five hours. The surface was greatly damaged which prevented the oxide measurement through ellipsometry. SEM imaging relvealed the extent of the damage, illustrated in Figure 38 and Figure 39. The contamination was measured by energy dispersive x-ray spectroscopy (EDAX). And it is shown in Figure 40.

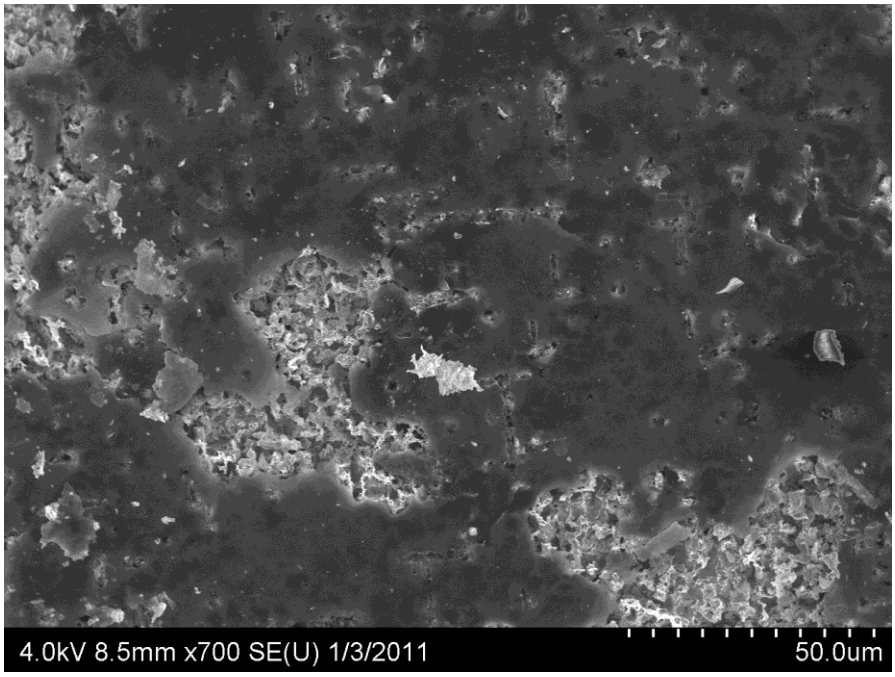


**Figure 38. Etching damage on an annealed Silicon sample after 5 hours in a nitrogen atmosphere. Extensive damage is evident.**

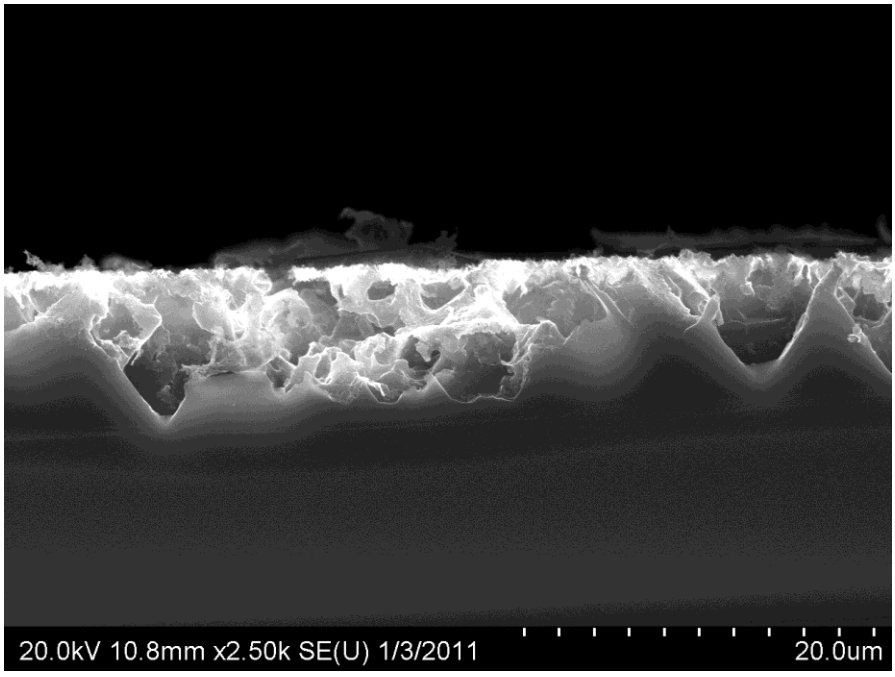


**Figure 39. Cross sectional view of the damage on an annealed silicon sample. Very high thermal etching can be observed.**

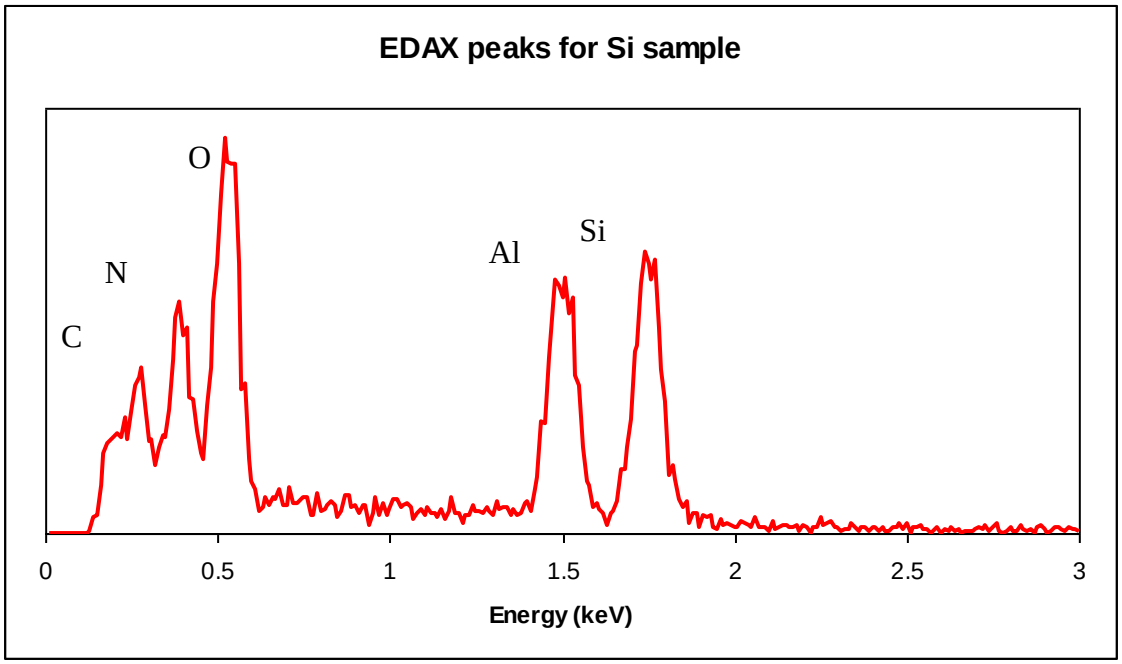


**Figure 40. Edax peaks for the Si sample. Various types of impurities are present.**

Thermal etching is explained as arising from both the long annealing time and from the presence of oxygen in the annealing atmosphere. The contaminants observed on the silicon sample through EDAX after the annealing was performed were carbon, nitrogen, oxigen and aluminum. Carbon probably come from contamination in the tube present before the annealing. Nitrogen comes directly from the annealing atmosphere, suggesting the posibility of silicon nitridation at high temperatures. Lastly, it is probable that the aluimina tube was the main source of contamination from both oxygen and aluminum. Samples annealed in hydrogen at lower temperatures and for shorter time suffered similar types of contamination and damage, sans nitrogen contamination.

In an attempt to eliminate the contamination and etching problems arising from the use of an alumina tube, a superalloy tube was suggested as a replacement. The superalloy chosen was an iron-nickel-chromium alloy known as RA-330. The composition of this alloy is presented in Table 5.

**Table 5. Chemical composition of the RA330 alloy.**

| Alloy | Min % | Max % |
|---|---|---|
| Chromium (Cr) | 18 | 20 |
| Nickel (Ni) | 34 | 37 |
| Silicon (Si) | 1 | 1.5 |
| Carbon (C) | — | 0.08 |
| Manganese (Mn) | — | 2 |
| Phosphorus (P) | — | 0.03 |
| Sulfur (S) | — | 0.03 |
| Copper (Cu) | — | 1 |
| Iron (Fe) | Balance | |

This alloy has very good oxidation resistance at up to 1200 °C, which is needed because the outer wall of the tube will be exposed to the regular atmosphere. It was designed to withstand quenching, which means that the temperature rate can be extremely high without the material fracturing due to thermal shock, and it has good resistance to hydrogen embrittlement.

While the material characteristics seem near ideal, two issues occurred when using this setup. First, as illustrated in Figure 41, silicon reacts with the alloy at high temperatures, which demands the use of an intermediate holder of boron nitride. The second and perhaps more important issue was the extremely high outgassing of material from the tube. this outgassing caused a chromium layer to form on the surface of silicon, which of course precludes its use in high temperature annealing. The resulting layer of chrome metal alloy is shown on Figure 42.

**Figure 41. Silicon has reacted with the alloy material.**

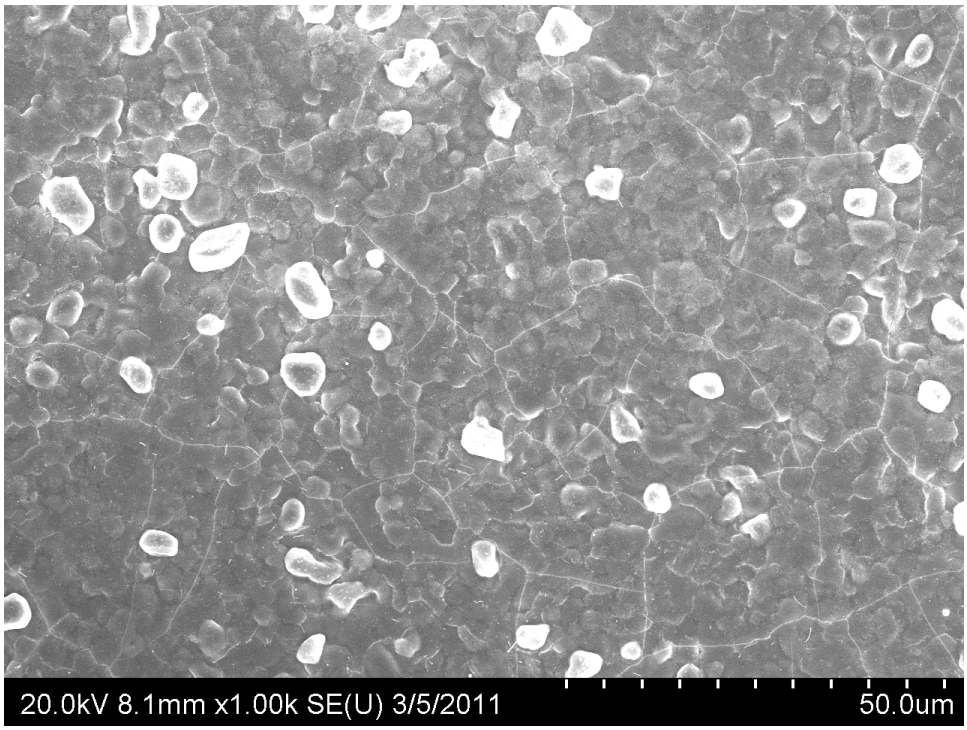


**Figure 42. Metallic grains deposited on the silicon surface after annealing for 30 minutes in a 5 Torr hydrogen atmosphere inside the RA330 tube.**

These experiments again demonstrated the need for a very clean annealing ambient, including the atmosphere and the materials exposed to very high temperature.

### *2.3.6 Annealing in a Custom Heating Chamber*

A custom heating chamber was built to provide the required annealing atmosphere for silicon reshaping. This chamber is capable of reaching a rough vacuum level of 40 mTorr, controllable up to 400 Torr with a nitrogen flow, and up to 10 Torr with hydrogen flow. The chamber is made out of various materials, but only the boron nitride heater, the pyrolityc graphite from the electrical contacts, and the tantalum conductors are exposed to the very high temperatures, minimizing the potential sources of contamination. The maximum temperature of the heater used is 1200 °C, and the temperature ramp rate can reach near 100 °C/min.

This setup, save for the vacuum level, closely resembles the conditions inside a CVD chamber such as the ones used in the literature for reshping of hydrogen. The completed setup is shown in Figure 43.

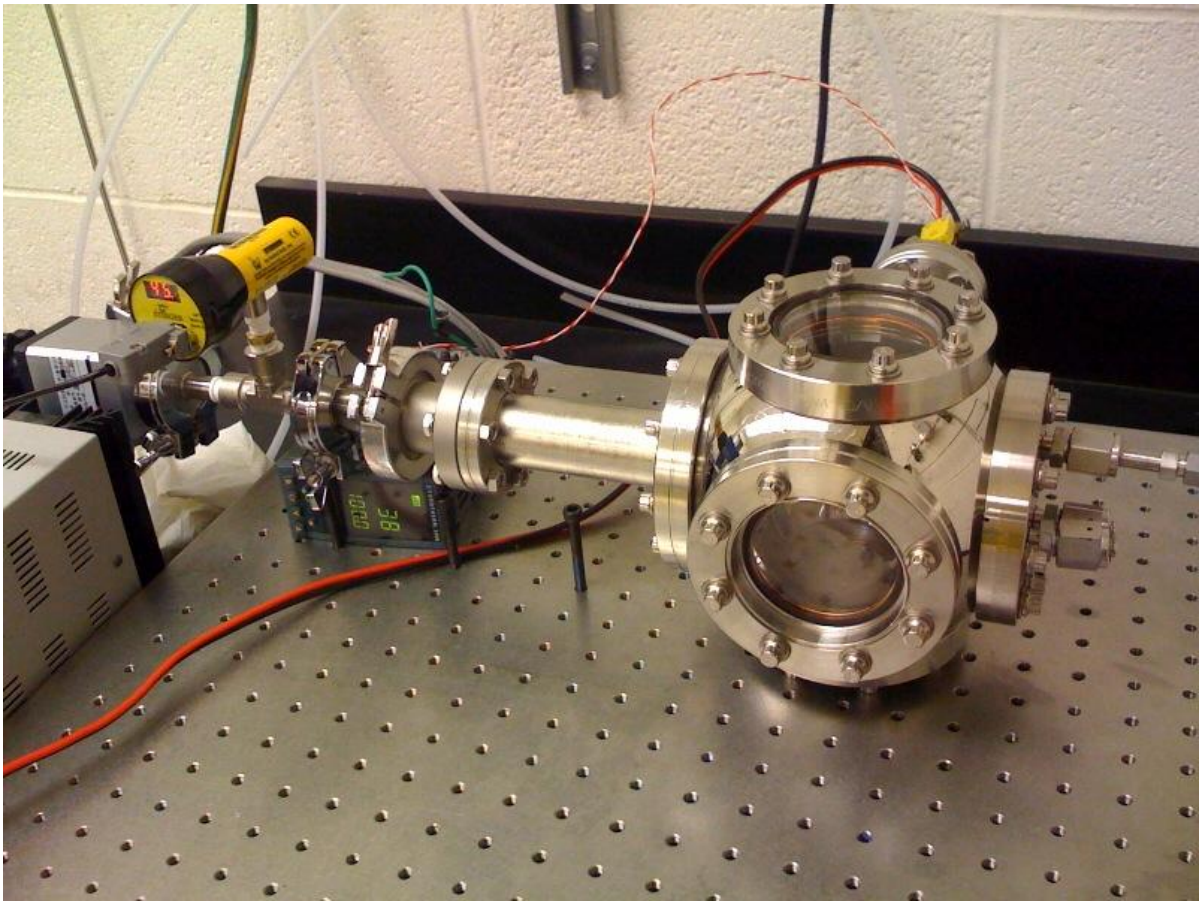

**Figure 43. Custom heating chamber.**

### *Procedure Used*

Both the sample and the silicon pieces used to hold the sample in place were cleaned for these experiments. The heater and associated high temperature parts were baked out at the maximum temperature for 1 hour once after installing the chamber, and the chamber was kept under vacuum to minimize the contamination.

**Sample cleaning.** The sample was cleaned as per the regular procedure in clean beakers and then transferred to a non-hermetic acrylic box where it remained for approximately 2 minutes before being inserted in the heating chamber.

1. Piranha – 5 minutes
   - 1 $H_2O_2$ : 2 $H_2SO_4$
2. DI water rinse
3. BOE – 1 minute
4. DI water rinse
5. Nitrogen dry

**Heating procedure**:

1. Sample placed in the furnace immediately after cleaning (2 minutes)
   - Placed centered directly on top of the Boron nitride heater. Two long silicon pieces were also used to ensure that the sample stays in place
   - The top flange is closed and the screws are tightened in a star shaped pattern.
   - Screws are tightened with a medium amount of torque
2. Vacuum pump is turned on and the chamber is purged with $N_2$
   - UHP $N_2$ flows into the chamber for 30 minutes before turning it on.
   - Flow set at 4 slpm.
   - Screws are fully tightened
3. Heater is turned on.
   - Annealing atmosphere is changed to the desired conditions
   - Temperature is controlled directly from the applied voltage
   - Target heating rate 50 °C/min
   - Target temperature between 1000 and 1300 °C
   - Dwell time between ½ and 1 hour
4. Sample is removed from the furnace when the chamber cools down and the temperature inside temperature reaches ~60 C

### *Results and Analysis*

Only preeliminary results are available for this chamber at the time. Initial results are shown in Figure 44. Oxidation was measured at around 1 nm, consistent with the thickness of the native oxide. It is unlikely that this oxide is present when the sample is being annealed because of the presene of hydrogen. Instead, the native oxide grows between the time when the sample is removed from the heating chamber and when the sample oxide is measured. No contamination could be measured or observed on this sample including through SEM and EDAX. It is suggested that a surface sensitive technique be used instead.

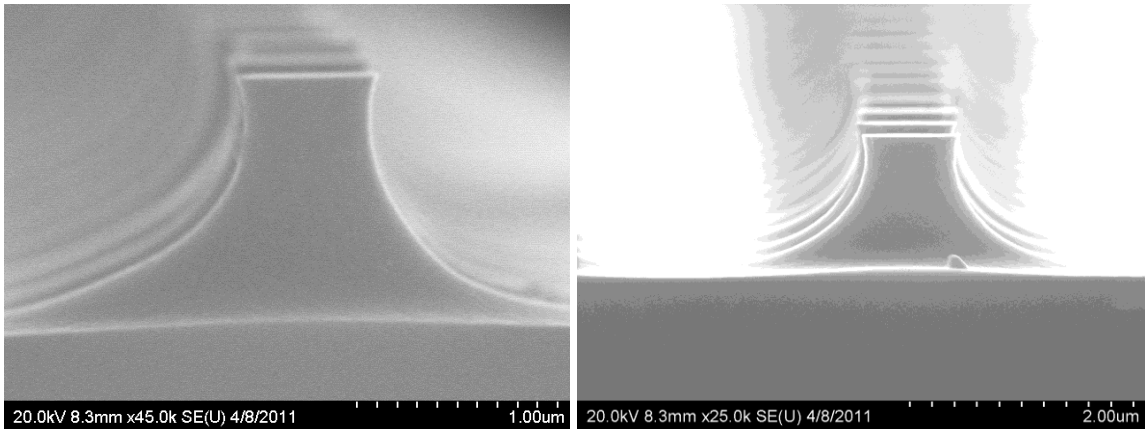


(a) (b)

**Figure 44. Silicon micropillars (a) before and (b) after annealing in the custom heating chamber under a 5 Torr hydrogen atmosphere for 30 minutes.**

Issues with the thermocouple prevented the proper measurement of the temperature in the sample. Instead, a piece of copper, whose melting temperature is 1050 °C, was annealed under the same conditions to observe the melting transition and form the basis of a calibration curve. The result from this experiment was that the copper did not melt, contrary to expectations. Therefore the annealed samples were not annealed at a temperature significant enough to produce the desired melting effect.

Improvements have been sugested to the current heating chamber to enable annealing at higher temperatures. First it was observed that the whole chamber heated up significantly when annealing samples, therefore a heat shield of molybdenum or tantalum is suggested as a way to alleviate the heat loss to the chamber walls. Second, changing the power supply to one with higher maximum voltage is a possibility, though direct current (DC) power supplies at voltages higher than 40 Volts that also deliver the required current are not common.

## 2.4 Annealing Simulation via MEMS Software

A MEMS chevron actuator was designed at the Universidad Autonoma de Ciudad Juarez (UACJ) with the purpose of reshaping (rounding) the actuation arms using joule heating. Figure 45 below shows the design of the MEMS chevron actuator.

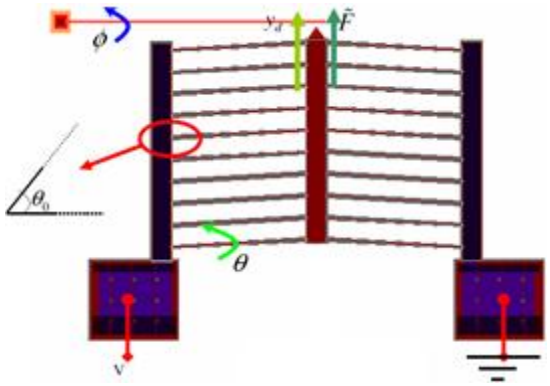


**Figure 45. Design of chevron actuator to study reshaping of silicon.**

Simulation using an equation of the form,

$$P_\Omega = J^2 \rho \eta \;=\; P_\Omega = (\frac{Vwh}{2\rho L})^2 (\frac{\rho L}{wh}) = \frac{V^2 wh}{4\rho L}$$

in Coventor software predicts that sufficient temperature (~1400 °C) can be achieved by applying an 11 Volt bias. This temperature is high enough to cause significant reshaping of the actuation arms and in the extreme case, melting. Results of simulation are shown in Figure 46. Lithography masks were fabricated to create the Chevron actuators on SOI wafers.

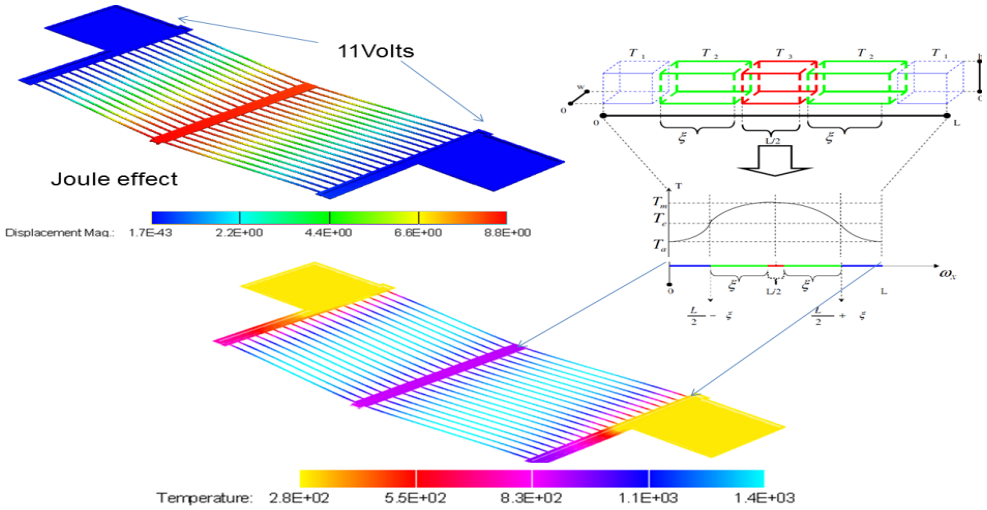


**Figure 46. Simulation of displacement and heating of actuation arms using Coventor software.**

## 2.5 Equipment Considerations

Safety is the most important consideration when using and designing equipment where hydrogen is involved. Two hydrogen detectors were used to ensure a both a leak free system, and the proper dilution of the exhausted gases. The handheld detector from H2SCAN, HY Alerta 500 (Figure 47), was used as a general leak detector and was used to inspect the hydrogen lines at every joint between the gas cylinder and the heating chamber.


**Figure 47. HY Alerta 500 handheld hydrogen leak detector.**

The exhaust, the laboratory roof, and the gas cabinet were continually monitored by the second hydrogen detector, a Scientific MIDAS from Honeywell Analytics (Figure 48) equipped with a

lower explosive limit (LEL) detection cartridge for hydrogen. The MIDAS has a gas inlet line with push in fittings so that a polyethylene or similar material tube can be used to connect the detector to the desired measurement point.

**Figure 48. Scientific Midas gas detector from Honeywell.**

Three measurement points were chosen for this detector and were automatically switched by a PIC 508 microcontroller interfaced with the corresponding three solenoid actuated valves. The schematic of the circuit used to control the valves is illustrated in Figure 49. And the code used on the microcontroller is presented in the appendix.

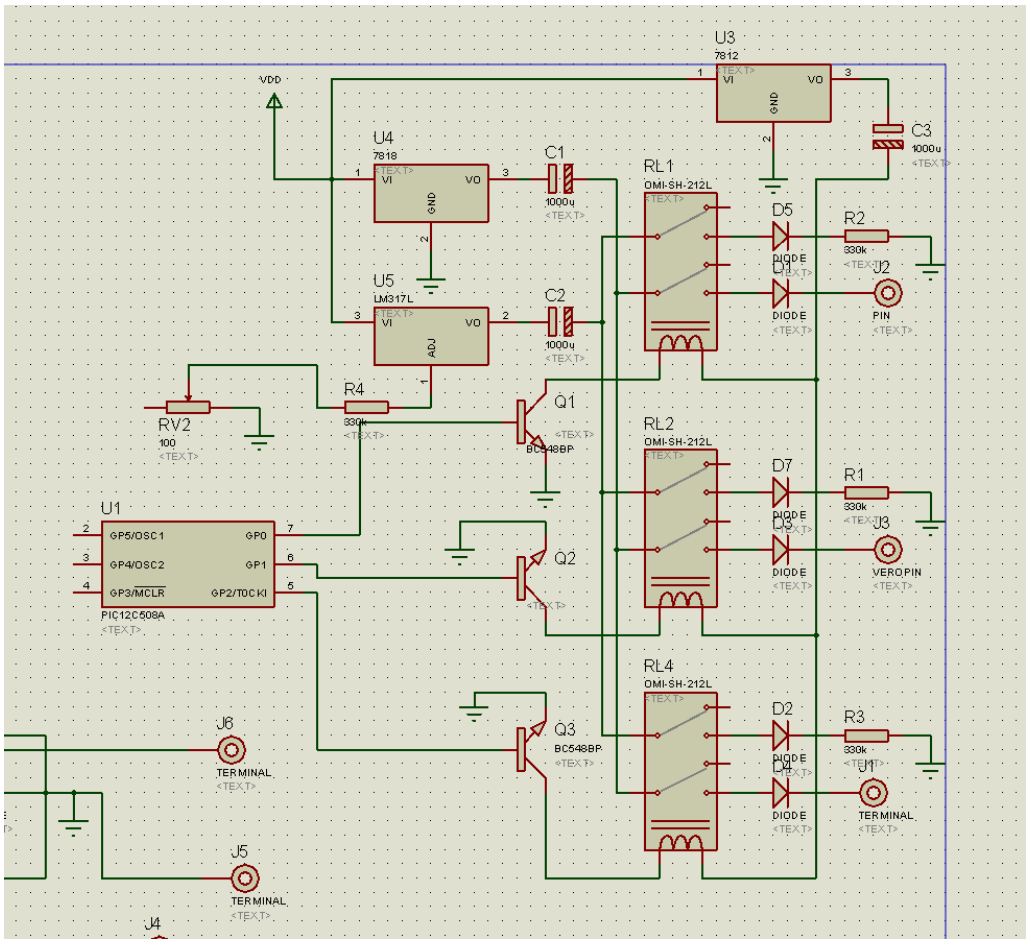


**Figure 49. Schematic for the solenoid controlled valves.**

The alarm from the MIDAS detector was wired to the remote input of the alarm for the electronic shutoff valve in the gas cabinet where the hydrogen is stored. This means that if the alarm goes off, the hydrogen gas cylinder is immediately isolated from the line. The gas cabinet used is similar to the one illustrated in Figure 50.

**Figure 50. Gas cabinet with alarm system for safe hydrogen storage.**

The same components were used to control the vacuum and the gas flow for both the MTI tube furnace, and the custom heating chamber. Vacuum was achieved with a Varian SH-100 dry scroll pump. For the most part, a dry scroll pump can safely pump pure hydrogen, as long as the seals are in good condition. Vacuum was controlled using a stainless steel vacuum bell valve. It was measured using a CVM-211 STINGER convection gauge calibrated for $N_2$

# 3. CONCLUSIONS

This project studied the reduced melting of *nano*-patterned silicon for microsystems applications such as for bonding of surfaces. The project also studied 3D morphological transformation of *micro*-patterned silicon. Reshaping, smoothing and rounding of silicon structures have useful applications in MEMS. For example, structures that are not accessible with traditional MEMS fabrication can be achieved using 3D morphological transformation of micro-patterned structures. A specific example is having round (instead of tubular) arms in a chevron actuator. Another example is the smoothing of rough surfaces via surface-melting of silicon at temperatures below the bulk melting point.

Extensive research capability was created at UTEP and UACJ including RIE, lithography, annealing, and design. This was required since the experimental capability did not exist for many of the processes including nanopatterning, dry etching, and annealing in an ultra-pure environment at temperatures in the ranges between 900 °C and 1400 °C. Some of the processing was performed at UT Austin and simulation at UACJ. This allowed systematic exploration.

Experiments were systematically performed to replicate the reduced melting point and 3D morphological transformation. Initial annealing results in a CVD reactor showed clear shape transformations, indicating melting, at temperatures ≥1000 °C. While these results are highly encouraging, replicating them proved quite challenging. Oxidation and oxygen contamination during anneal was the main issue. Extensive work was performed to address this issue including testing different types of annealing apparatus including; a box furnace, a quartz tube furnace, a ceramic tube furnace, a metal tube furnace, a high-vacuum heating stage in an x-ray diffraction (XRD), and a custom heating chamber. It was determined that the issue can be addressed by using a hermetically sealed heating chamber and by minimizing or eliminating altogether the presence of oxygen containing materials in the heated area. Thermal etching is similarly addressed by eliminating the sources of oxygen in the heating chamber, and by using a high temperature ramp, since thermal etching is a significantly slower effect than reshaping. The information derived from these experiments was used to design a custom heating chamber in which reshaping can be explored. Initial results from this custom heating chamber revealed no change in morphology but also no contamination on the samples. Although, these results were encouraging, the temperature was not high enough to see the effect of shape transformation.

A total of 4 students were supported including graduation of 1 master and 1 baccalaureate students during the period. The master student successfully presented his master's thesis.

Results from this project were presented at the 2010 Commercialization of MEMS conference (COMMS) in Albuquerque, NM on August 30$^{th}$.

In summary, this project created research capacity at UTEP, mentored 4 students and graduated two, produced a master's thesis and, strengthened collaborations with UACJ in Mexico.

# 4. REFERENCES


1. J. M. Blakely, *Introduction to the Properties of Crystal Surfaces*, Pergamon Press, Oxford, Chapter 1 (1973).
2. J. M. Howe, *Interfaces in Materials*, John Wiley & Son, Inc., New York, Chapter 3 (1997).
3. D. Zubia, Unpublished. This equation is based on the discussions by J. M. Howe, *Interfaces in Materials*, John Wiley & Son, Inc., New York, 1997, and J. M. Blakely, *Introduction to the Properties of Crystal Surfaces*, Pergamon Press, Oxford, 1973.
4. C. Herring, "Some theorems on the free energies of crystal surfaces," *Phys. Rev.* **82**, 87 (1951).
5. D. J. Srolovitz, "On the stability of surfaces of stressed solids," *Acta metall.* **37**, p. 621 (1989).
6. S. J. Peppiatt and J. R. Sambles, "The melting of small particles. I. Lead," *Proc. R. Soc. Lond. A.* **345**, 387 (1975).
7. Ph. Buffat and J-P. Borel, "Size effect on the melting temperature of gold particles" , *Phys. Rev. A* **13**, 2287 (1976).
8. A. Goldstein, *Handbook of nanophase materials*, Marcel Dekker, New York, pp. 3-4 (1997).
9. S. H. Zaidi, A. S. Chu, and S. R. J. Brueck, "Scalable fabrication and optical characterization of nm Si structures," *Mat. Res. Soc. Symp. Proc.* **358**, 957 (1995).
10. S. H. Zaidi, A. S. Chu, and S. R. J. Brueck, "Optical properties of nanoscale, one-dimensional silicon grating structures," *J. Appl. Phys. **80**, 6997* (1996).

# DISTRIBUTION

3 Department of Electrical and Computer Engineering *(electronic copies)*
Attn: David Zubia
Stella Quinones
Noel Marquez
University of Texas at El Paso
El Paso, TX 79968

1 Jose Mireles *(electronic copy)*
Instituto de Ingenriería y Tecnología
Universidad Autónoma de Ciudad Juárez
Ciudad Juárez, Mexico

| | | | |
|---|---|---|---|
| 1 | MS0359 | D. Chavez, LDRD Office | 1911 *(electronic copy)* |
| 1 | MS0899 | RIM-Reports Management | 9532 *(electronic copy)* |


Sandia National Laboratories